Published for SISSA by Springer

Received: May 10, 2016
Accepted: June 6, 2016
Published: June 17, 2016

Λ scattering equations

Humberto Gomez

Instituto de Fisica — Universidade de São Paulo,
Caixa Postal 66318, 05315-970 São Paulo, SP, Brazil
Facultad de Ciencias Basicas, Universidad Santiago de Cali,
Calle 5 N° 62-00 Barrio Pampalinda, Cali, Valle, Colombia

E-mail: humgomzu@gmail.com

Abstract: The CHY representation of scattering amplitudes is based on integrals over the moduli space of a punctured sphere. We replace the punctured sphere by a double-cover version. The resulting scattering equations depend on a parameter Λ controlling the opening of a branch cut. The new representation of scattering amplitudes possesses an enhanced redundancy which can be used to fix, modulo branches, the location of four punctures while promoting Λ to a variable. Via residue theorems we show how CHY formulas break up into sums of products of smaller (off-shell) ones times a propagator. This leads to a powerful way of evaluating CHY integrals of generic rational functions, which we call the Λ algorithm.

Keywords: Differential and Algebraic Geometry, Scattering Amplitudes, Superstrings and Heterotic Strings, Field Theories in Higher Dimensions

ArXiv ePrint: 1604.05373

Open Access, © The Authors.
Article funded by SCOAP[3].

doi:10.1007/JHEP06(2016)101

JHEP06(2016)101

Contents

1 Introduction **2**

2 Preliminaries **4**
- 2.1 CHY construction 4
- 2.2 Examples 5
- 2.3 Singularities on $\mathcal{M}_{0,n}$ 7

3 Double-cover formulation **7**
- 3.1 Redundancies 9
  - 3.1.1 Promoting Λ to variable 10
- 3.2 Equivalence with the CHY construction 11

4 New gauge fixing **12**
- 4.1 New gauge fixing 13

5 Residue theorem and diagrammatic expansion **13**
- 5.1 Residue theorem 14
- 5.2 Recovering the curve 15

6 Λ-diagrams and a new algorithm **17**
- 6.1 More notations and a simple example 18
  - 6.1.1 Configurations and Λ-theorem 19
- 6.2 The Λ-algorithm 21
- 6.3 Building blocks 24
  - 6.3.1 General KLT algorithm and computation of the (V) building block 25

7 Examples **27**
- 7.1 Six-point 27
  - 7.1.1 $\mathcal{I}_{(\mathcal{A})}$-computation 27
  - 7.1.2 $\mathcal{I}_{(\mathcal{B})}$-computation (general KLT and Λ algorithms) 31
- 7.2 Eight-point 34

8 The Baadsgaard, Bohr, Bourjaily and Damgaard Rules (BBBD) vs the Λ-algorithm **37**

9 Discussions **39**

A Λ-theorem **41**

JHEP06(2016)101

1 Introduction

The complete tree-level S-matrix of a large variety of field theories of massless particles are now known (or conjectured) to have a description in terms of contour integrals over $\mathcal{M}_{0,n}$, the moduli space of n-punctured Riemann sphere [1–13]. Some of these theories are Yang-Mills, Einstein gravity, Dirac-Born-Infeld, and the U(N) non-linear sigma model [3, 12]. The new formulas for the scattering of n particles are given as a sum over multidimensional residues [14] on $\mathcal{M}_{0,n}$.

In addition, many algorithms have been created in order to compute these kind of contour integrals [15–25], as well as much progress have been done at loop level [7, 26–35].

Denoting the position of n punctures on a sphere by $\{z_1, z_2, \dots z_n\}$ and using $\mathrm{PSL}(2,\mathbb{C})$ to fix three of them, say z_1, z_2, z_3, there is a rational map from $\mathbb{C}^{n-3} \to \mathbb{C}^{n-3}$ which is a function of the space of kinematic invariants for the scattering of n massless particles ($k_a^2 = 0$), $s_{ab} = k_a \cdot k_b$,

$$E_a(z) = \sum_{b=1, b\neq a}^{n} \frac{s_{ab}}{z_a - z_b}, \quad \text{for} \quad a \in \{1, 2, \dots, n\}, \tag{1.1}$$

with $a \in \{4, 5, \dots, n\}$.

Using this map scattering amplitudes are defined as the sum over the residues of

$$\mathcal{M}_n = \int d^{n-3}z \frac{|1,2,3|^2\ H(z)}{E_4(z)E_5(z)\cdots E_n(z)}. \tag{1.2}$$

over all the zeroes of the map $\{E_4, E_5, \dots, E_n\}$. Here $|1,2,3| = (z_1 - z_2)(z_2 - z_3)(z_3 - z_1)$ and $H(z)$ is a rational function that depends on the theory under consideration. The equations defining the zeroes, $E_a = 0$, are known as the scattering equations [36–44]. In section 2 we will give a short review about this ideas.

The representation (1.2) of scattering amplitudes makes many properties manifest. Some of them are gauge invariance, soft limits, BCJ relations and the existence of KLT formulas [17, 45–55]. The drawback is that integrals of the form (1.2) require the solution of polynomial equations whose degree increases with the number of particles.

In this paper we reformulate the formula for scattering amplitudes in terms of a double cover of the punctured sphere. More precisely, we consider a sphere as a curve in $\mathbb{C}P^2$ defined by

$$y^2 = \sigma^2 - \Lambda^2, \tag{1.3}$$

where Λ is a non zero constant parameter. Clearly, the curve is invariant under a simultaneous scaling of the coordinates (y, σ, Λ). The new formulation is schematically given by

$$\mathcal{M}_n = \frac{1}{\mathrm{Vol}(\mathrm{PSL}(2,\mathbb{C}))} \int \prod_{a=1}^{n} \left(\frac{(y_a\, dy_a)}{\prod_{a=1}^{n}(y_a^2 - \sigma_a^2 + \Lambda^2)} \right) \prod_{b=1}^{n} \frac{d\sigma_b\ H(\sigma, y, \Lambda)}{E_b(\sigma, y, \Lambda)}. \tag{1.4}$$

Integration over both residues of the curve implements the sums over choices of branches.

JHEP06(2016)101

In the double cover description each puncture is specified by a pair of complex numbers (σ_a, y_a). The value of y_a indicates the branch where the puncture is located. The new form of the components of the map E_a is

$$E_a(\sigma, y, \Lambda) = \sum_{b=1, b\neq a}^{n} \frac{1}{2}\left(\frac{y_b}{y_a} + 1\right) \frac{s_{ab}}{\sigma_a - \sigma_b}. \tag{1.5}$$

This form is very easy to motivate and it is done in section 3.

The differential form being integrated in the double cover version of the formula for $\mathcal{M}_n$ is invariant under the global rescaling inherited from $\mathbb{C}P^2$. This $\mathbb{C}^*$ group can be promoted to a full redundancy of the description introducing the scale measure

$$\frac{1}{\text{vol}(\mathbb{C}^*)} \frac{d\Lambda}{\Lambda}, \tag{1.6}$$

where the Λ factor is proportional to the square root of the discriminant of the quadratic curve in (1.3), $\Delta = 4\Lambda^2$. The $\mathbb{C}^*$ action is non-trivial on the puncture locations, this means that one can combine the new $\mathbb{C}^*$ action with the $\text{PSL}(2, \mathbb{C})$ group of the sphere and use it to fix the σ coordinate of four punctures. Doing so leaves Λ as an integration variable to be fixed by the scattering equations. This is done in section 4.

In section 5 we show that the global residue theorem can be used to replace one of the components of the map, say E_n, by Λ. As it turns out the residue theorem only picks up poles at $\Lambda = 0$ and at $\Lambda = \infty$ and both are identical. At $\Lambda = 0$ the branch cut connecting the two branches of the double cover closes and the integrals separates into sectors. Each sector is determined by the distribution of the punctures between the two branches. The amplitude then becomes schematically

$$\mathcal{M}_n = \sum_{U \cup D} \mathcal{M}_U^{\text{off}-\text{shell}} \frac{1}{P_U^2} \mathcal{M}_D^{\text{off}-\text{shell}}. \tag{1.7}$$

where the sum is over possible distributions of punctures and $\mathcal{M}^{\text{off}-\text{shell}}$ refers to amplitudes where one particle, corresponding to the puncture created by the closing of the branch cut is off-shell.

We apply this procedure to more general integrals over the moduli space which appear as parts of physical amplitudes in their CHY representation. In these more general cases, when the integrand has at most double poles on the boundary of the moduli space $\mathcal{M}_{n,0}$ then the propagator is a standard Feynman propagator. An example of an integral with at most double poles is

$$\int d^n z \frac{1}{E_1(z) E_2(z) \cdots E_n(z)} \frac{1}{(123\cdots n)^2} \tag{1.8}$$

where

$$(123\cdots n) := (z_1 - z_2)(z_2 - z_3)\cdots(z_n - z_1). \tag{1.9}$$

This integral is known to give the sum over all Feynman diagrams computing a partial amplitude in a cubic scalar theory in the bi-adjoint representation of $\text{U}(N) \times \text{U}(M)$. Iterating the procedure gives rise to a novel set of diagrams where the buliding blocks are four-particle amplitudes and propagators.

JHEP06(2016)101

When the integrand has higher order poles on the moduli space one finds generalized propagators which are made from higher powers of kinematic invariant. One example, explicitly compute in section 6, is a six-particle integral

$$\int d^6 z \frac{1}{E_1(z)E_2(z)\cdots E_6(z)} \frac{1}{(1234)^2(56)^2} \tag{1.10}$$

with $(56) = (z_5 - z_6)(z_6 - z_5)$ consistent with the definition (1.9). This integral has poles of the form $1/s_{56}^3$.

A very familiar way of understanding this process is by analogy with the Stukelberg procedure for taking massless limits of massive vector bosons [56]. The mass parameter is played by the kinematic invariant controlling the factorization limit while the Stukelberg field is played by the Λ parameter. All this process is shown in section 6, where we formulate a new algorithm and in section 7 we give three non trivial examples.

In section 8 we compare our method with the rules given in [18] by Baadsgaard et al. We also generalize the new algorithm to non trivial numerators and we give a simple example.

Finally, we end in section 9 with discussions.

2 Preliminaries

In this section we review the basic CHY construction [1–3] and show some examples that motivate the double-cover construction.

2.1 CHY construction

Consider the scattering of n massless particles. The scattering data is determined in terms of a set of n momentum vectors $\{k_1^\mu, k_2^\mu, \ldots, k_n^\mu\}$ and n wave functions $\{\epsilon_1^\mu, \epsilon_2^\mu, \ldots, \epsilon_n^\mu\}$. Here we take the wave functions to be polarization vectors as higher spin wave functions, e.g. for gravitons, can be constructed using tensor products. In a slightly different terminology from the original CHY construction, one introduces n rational functions of the puncture locations, z_a, defined by [1, 39]

$$E_a = \sum_{b=1, b\neq a}^{n} \frac{s_{ab}}{z_a - z_b}. \tag{2.1}$$

It is easy to show that three linear combinations vanish

$$\sum_{a=1}^{n} z_a^m E_a = 0 \quad \text{for} \quad m \in \{0, 1, 2\}. \tag{2.2}$$

Recalling that different configurations of punctures on a $\mathbb{C}P^1$ are to be identified if they differ by a $\mathrm{PSL}(2, \mathbb{C})$ transformation. This means that the location of three punctures can be fixed. It is possible to show that for any rational function $H(z)$ which transforms as

$$H(z) \to H(z) \prod_{a=1}^{n} (\gamma z_a + \delta)^4, \quad \text{when} \quad z_a \to \frac{\alpha z_a + \beta}{\gamma z_a + \delta} \quad \text{and} \quad \alpha\delta - \beta\gamma = 1, \tag{2.3}$$

JHEP06(2016)101

the contour integral [1]

$$\int \prod_{a=1,a\neq\{i,j,k\}}^{n} dz_a \frac{|ijk|_z |pqr|_z}{\prod_{c=1,c\neq\{p,q,r\}}^{n} E_c(z)} H(z) \tag{2.4}$$

that computes one of the local residues at a zero of the map $\mathbb{C}^{n-3} \to \mathbb{C}^{n-3}$ is independent of the choice of fixed punctures $\{z_i, z_j, z_k\}$ and of equations eliminated $\{E_p, E_q, E_r\}$ to construct the map. In this formula $|ijk|$ stands for the Vandermonde determinant of z_i, z_j, z_k.

One way to see that this is the case is to realize that the generators of $\mathrm{PSL}(2,\mathbb{C})$ are

$$L_1 = \sum_{a=1}^{n} \partial_{z_a}, \quad L_0 = \sum_{a=1}^{n} z_a \partial_{z_a}, \quad L_{-1} = \sum_{a=1}^{n} z_a^2 \partial_{z_a}. \tag{2.5}$$

Treating the $\mathrm{PSL}(2,\mathbb{C})$ as a redundance of the integral and using a gauge fixing procedure one can check that the Fadeev-Popov determinant is indeed

$$|ijk|_z = \begin{vmatrix} 1 & z_i & z_i^2 \\ 1 & z_j & z_j^2 \\ 1 & z_k & z_k^2 \end{vmatrix}. \tag{2.6}$$

2.2 Examples

The CHY representation of many theories are known (or are conjectured). In this subsection we review some of them in order to motivate the constructions in this paper.

Let us start with Einstein gravity [1, 2]. The integrand H is computed as the reduced determinant of a matrix a $2n \times 2n$ antisymmetric matrix

$$\Psi = \begin{pmatrix} A & -C^{\mathrm{T}} \\ C & B \end{pmatrix}, \tag{2.7}$$

where A, B and C are $n \times n$ matrices. The first two matrices have components

$$A_{ab} = \begin{cases} \dfrac{k_a \cdot k_b}{z_a - z_b} & a \neq b, \\ 0 & a = b, \end{cases} \qquad B_{ab} = \begin{cases} \dfrac{\epsilon_a \cdot \epsilon_b}{z_a - z_b} & a \neq b, \\ 0 & a = b, \end{cases} \tag{2.8}$$

while the third is given by

$$C_{ab} = \begin{cases} \dfrac{\epsilon_a \cdot k_b}{z_a - z_b} & a \neq b, \\ -\displaystyle\sum_{c=1;c\neq a}^{n} \dfrac{\epsilon_a \cdot k_c}{z_a - z_c} & a = b. \end{cases} \tag{2.9}$$

This matrix depends on the momenta k_a^μ and on polarization vectors ϵ_a^μ.

The diagonal components of the C matrix can be written in a manifestly $\mathrm{PSL}(2,\mathbb{C})$ covariant way by choosing a momentum vector, say k_n if $a \neq n$, and eliminating it using momentum conservation

$$C_{aa} = -\sum_{b=1,b\neq a}^{n-1} \epsilon_a \cdot k_c \frac{(z_n - z_c)}{(z_a - z_c)(z_a - z_n)}. \tag{2.10}$$

JHEP06(2016)101

The integrand is given by

$$H^{\text{gravity}}(z) = \det{}'\Psi = \frac{1}{(z_i - z_j)^2} \det \Psi^{ij}_{ij}, \tag{2.11}$$

where Ψ^{ij}_{ij} is the $(n-2)\times(n-2)$ matrix obtained from Ψ by removing the rows (i,j) and the columns (i,j).

The second example is that of the scattering of gluons in a U(N) Yang-Mills theory [1, 2]. The coefficient of the trace $\text{Tr}(T^{a_1}T^{a_2}\cdots T^{a_n})$ is computed by the integrand

$$H^{\text{YM}}(z) = \frac{1}{(123\cdots n)} \text{Pf}'\Psi, \tag{2.12}$$

where $\text{Pf}'\Psi = (z_i - z_j)^{-1}\text{Pf}\Psi^{ij}_{ij}$ and $(123\cdots n) = (z_1 - z_2)(z_2 - z_3)\cdots(z_n - z_1)$.

The third example is that of a scalar theory in the bi-adjoint representation of U(N) $\times$ U($\tilde{N}$) [2]. The coefficient of the trace $\text{Tr}(T^{a_1}T^{a_2}\cdots T^{a_n})\text{Tr}(\tilde{T}^{a_{w(1)}}\tilde{T}^{a_{w(2)}}\cdots\tilde{T}^{a_{w(n)}})$ with w some permutation of labels, is given by

$$H^{\text{scalar}}(z) = \frac{1}{(123\cdots n)} \times \frac{1}{(w(1)w(2)w(3)\cdots w(n))}. \tag{2.13}$$

The last two examples are also purely scalar theories but with derivative interactions [3, 11].

The fourth example is a special Galileon theory (sGal) that possesses more non-linearly realized symmetries than a generic Galileon. Amplitudes in this theory are computed using

$$H^{\text{sGal}}(z) = \left(\det{}'A\right)^2, \tag{2.14}$$

where $\det'A = (z_i - z_j)^{-2}\det A^{ij}_{ij}$.

The fifth and final example is the U(N) non-linear sigma model. The term proportional to the trace $\text{Tr}(T^{a_1}T^{a_2}\cdots T^{a_n})$ is computed by

$$H^{\text{NLSM}}(z) = \frac{1}{(123\cdots n)} \det{}'A, \tag{2.15}$$

In order to illustrate the kind of integrals we are interested in performing let us consider $\det'A$ for four particles,

$$\det{}'A_4 = \frac{1}{(z_1 - z_2)^2} \begin{vmatrix} 0 & \frac{s_{34}}{z_3 - z_4} \\ \frac{s_{34}}{z_4 - z_3} & 0 \end{vmatrix}. \tag{2.16}$$

This means that the integrands of the Galileon and NLSM are

$$H_4^{\text{sGal}} = s_{34}^4 \times \frac{1}{(z_1 - z_2)^4(z_3 - z_4)^4}, \quad H_4^{\text{NLSM}} = s_{34}^2 \times \frac{1}{(1234)} \frac{1}{(z_1 - z_2)^2(z_3 - z_4)^2}. \tag{2.17}$$

JHEP06(2016)101

2.3 Singularities on $\mathcal{M}_{0,n}$

The examples given above make it clear that a variety of integrands $H(z)$ can appear. One way to classify them is by the kind of singularities they have as different boundaries on the moduli space of a punctured sphere are approached. The largest codimension singularities are when two punctures approach each other. Consider for example the integrands for four particles [2, 3, 11]

$$H_4^{\phi^3} \sim \frac{1}{(1234)^2}, \quad H_4^{\text{NLSM}} \sim \frac{1}{(1234)} \frac{1}{(z_1-z_2)^2(z_3-z_4)^2}, \quad H_4^{\text{sGal}} \sim \frac{1}{(z_1-z_2)^4(z_3-z_4)^4}.$$

Clearly, the first integrand has double poles as any two consecutive punctures approach each other $z_a \to z_{a+1}$ and no other poles. The second integrand has a triple poles when $z_1 \to z_2$ and when $z_3 \to z_4$ and simple poles when $z_2 \to z_3$ and when $z_4 \to z_1$. Finally, the last integrand only has fourth order poles when $z_1 \to z_2$ and when $z_3 \to z_4$. It is easy to show that the order of the pole is related to the order of the propagator associated to the coincident punctures. If the integrand as a $(m+1)^{\text{th}}$ order pole when $z_a \to z_b$ then the integral has a pole of the form $1/s_{ab}^m$.

In the rest of this paper we develop a double cover formulation which is tailored for exploiting the behavior of integrands near boundaries of the moduli space. This method not only becomes a powerful tool in the evaluation of integrals but it also makes physical properties manifest such as crossing and factorization.

3 Double-cover formulation

We consider a sphere as a curve in $\mathbb{C}P^2$ defined by [14]

$$y^2 = \sigma^2 - \Lambda^2. \tag{3.1}$$

We call this curve Σ and it can be interpreted as two sheets joined by a branch cut. We take σ as the coordinate on a sheet and y as the variable determining the branch. Λ is taken to be a constant parameter that controls the opening of the branch cut joining the branch points $\sigma = -\Lambda$ and $\sigma = \Lambda$.

The location of n-punctures on Σ is given by n pairs $\{(\sigma_a, y_a)\}$. We would like to find formulation of the maps E_a defining the scattering equations for this curve. Clearly, E_a must have a simple pole when puncture a coincides with puncture b. On Σ, it is not enough to have $\sigma_a \to \sigma_b$ but we also need $y_a \to y_b$, i.e., they must be on the same branch. When $\sigma_a \to \sigma_b$ one can have either $y_a \to y_b$ or $y_a \to -y_b$. So we need a projector, $P_b^{(a)}$, that gives one in the former and zero in the latter. One choice is

$$P_b^{(a)} = \frac{1}{2}\left(\frac{y_b}{y_a} + 1\right). \tag{3.2}$$

This turns out to be the correct choice and one has

$$E_a(\sigma, y) = \sum_{b=1, b\neq a}^{n} \frac{1}{2}\left(\frac{y_b}{y_a} + 1\right) \frac{s_{ab}}{\sigma_a - \sigma_b}. \tag{3.3}$$

JHEP06(2016)101

One important condition the equations have to satisfy is that they must be covariant under the exchange of σ and y (with $\Lambda \to i\Lambda$) which is a symmetry of the curve Σ. It is easy to check that on the support of $y_b^2 = \sigma_b^2 - \Lambda^2$, the function $y_a E_a$ is invariant.

Having found the new version of the maps E_a which give rise to the scattering equations, the next step is to translate the rational function $H(z)$ which defines the theory under consideration. All such functions can be decomposed as linear combinations of functions of the form [17]

$$H(z) = \frac{1}{(\alpha(1)\alpha(2)\cdots\alpha(n))(\gamma(1)\gamma(2)\cdots\gamma(n))} f(r_{ijkl}), \tag{3.4}$$

where $(\alpha(1)\alpha(2)\cdots\alpha(n))$ and $(\gamma(1)\gamma(2)\cdots\gamma(n))$ are Parke-Taylor factors with ordering α and γ (see (1.9) for the Parke-Taylor factor definition [57]). f is a rational function of r_{ijkl} which are general cross ratios, i.e.,

$$r_{ijkl} \equiv \frac{z_{ij}\, z_{kl}}{z_{il}\, z_{jk}}, \tag{3.5}$$

where we have introduced a convenient shorthand notation

$$z_{ab} \equiv z_a - z_b \qquad (\sigma_{ab} \equiv \sigma_a - \sigma_b). \tag{3.6}$$

In order to map $H(z)$ to $H(\sigma, y)$, we define any combinations of factors of the form

$$(z_{a_1} - z_{a_2})(z_{a_2} - z_{a_3})\cdots(z_{a_{m-1}} - z_{a_m})(z_{a_m} - z_{a_1}) \tag{3.7}$$

as a chain $(a_1\ a_2\ \cdots a_{m-1}\ a_m)$ of length m. Chains are taken to have lengths $2 \le m \le n$. A chain of length 2 is given by

$$(a_1\ a_2) = (z_{a_1} - z_{a_2})(z_{a_2} - z_{a_1}). \tag{3.8}$$

It is straightforward to check

$$r_{ijkl} \equiv \frac{z_{ij}\, z_{kl}}{z_{il}\, z_{jk}} = \frac{z_{ij} z_{jl} z_{lk} z_{ki}}{z_{kj} z_{jl} z_{li} z_{ik}} = \frac{(ijlk)}{(ikjl)}. \tag{3.9}$$

Now we propose to use the following replacement into the chain so as to construct the integrand $H(\sigma, y)$,

$$\frac{1}{z_{ab}} \ \mapsto\ \tau_{a:b} \equiv \frac{1}{2}\left(\frac{y_a + y_b + \sigma_{ab}}{y_a}\right)\frac{1}{\sigma_{ab}}. \tag{3.10}$$

Note that while the left hand side is antisymmetric in the a and b labels the right hand side is not and hence the notation $\tau_{a:b}$. This fact becomes irrelevant when the substitution is made into chains and hence the importance of the appearance of them in the integrands. So, we complete the map $H(z) \to H(\sigma, y)$ by

$$H(\sigma, y) = (\tau_{\alpha(1):\alpha(2)}\cdots\tau_{\alpha(n):\alpha(1)})(\tau_{\gamma(1):\gamma(2)}\cdots\tau_{\gamma(n):\gamma(1)}) f\left(\frac{\tau_{i:k}\tau_{k:j}\tau_{j:l}\tau_{l:i}}{\tau_{i:j}\tau_{j:l}\tau_{l:k}\tau_{k:i}}\right). \tag{3.11}$$

JHEP06(2016)101

In addition one can check, in a simple way, the chain property

$$(a_1\, a_2 \cdots a_{m-1}\, a_m) = (-1)^m (a_m\, a_{m-1} \cdots a_2 a_1), \tag{3.12}$$

$$(\tau_{a_1:a_2} \cdots \tau_{a_{m-1}:a_m}\, \tau_{a_m:a_1}) = (-1)^m (\tau_{a_m:a_{m-1}}\, \tau_{a_{m-1}:a_{m-2}} \cdots \tau_{a_2:a_1}\, \tau_{a_1:a_m}), \tag{3.13}$$

and the inverse map works in the same way, $\tau_{a:b} \to \frac{1}{z_{ab}}$.

Moreover, it is straightforward to check the scattering equations can be written as

$$E_a(\sigma, y) = \sum_{b\neq a}^{n} s_{ab}\, \tau_{a:b} = \frac{1}{y_a} \sum_{b\neq a}^{n} s_{ab}\, \tilde{\tau}_{a:b} = \frac{1}{y_a} \tilde{E}_a(\sigma, y), \tag{3.14}$$

where we have denoted $\tilde{\tau}_{a:b}$ and $\tilde{E}_a$ as

$$\tilde{\tau}_{a:b} = \frac{y_a + y_b + \sigma_{ab}}{2\,\sigma_{ab}}, \qquad \tilde{E}_a = \sum_{b\neq a}^{n} s_{ab}\, \tilde{\tau}_{a:b}. \tag{3.15}$$

It is not obvious how chains appear in integrands that are computed using the Pfaffian or the determinant of the matrices Ψ of A.

3.1 Redundancies

Next we move to the discussion of the redundancies and how to gauge fix them. This subsection is only the first part of the discussion in which we show how to perform the standard gauge fixings. In the second part, presented in section 4, we perform a different gauge fixing which allow us to use residue theorems to break up contour integrals into integrals with smaller number of punctures.

We consider the following integral

$$\mathcal{I} = \frac{1}{\mathrm{Vol}(\mathrm{PSL}(2,\mathbb{C}))} \int \prod_{a=1}^{n} \frac{d\sigma_a\, (y_a\, dy_a)}{(y_a^2 - \sigma_a^2 + \Lambda^2)} \times \frac{H(\sigma, y)}{\prod_{b=1}^{n} E_b(\sigma, y)} \tag{3.16}$$

where Λ is a non-zero constant parameter and $H(\sigma, y)$ is a general rational function as in (3.11). The factor $\mathrm{Vol}(\mathrm{PSL}(2,\mathbb{C}))$ in the integral is there only as a reminder that the integral has a redundancy that has to be gauge fixed. The $\mathrm{PSL}(2,\mathbb{C})$ action is generated by the vectors (on the support of the algebraic curve $y_a^2 = \sigma_a^2 - \Lambda^2$, $a = 1, \cdots n$)

$$L_{\pm 1} = \sum_{a=1}^{n} \frac{1}{\Lambda} y_a (\sigma_a \mp y_a) \partial_a, \qquad L_0 = \sum_{a=1}^{n} y_a \partial_a, \tag{3.17}$$

where $\partial_a \equiv \partial/\partial\sigma_a$ and they satisfy the algebra

$$[L_{\pm 1}, L_0] = \pm\, L_{\pm 1}, \qquad [L_1, L_{-1}] = 2 L_0. \tag{3.18}$$

The covariance of the E_a maps under these transformations imply that there are three linear combinations among them

$$\sum_{a=1}^{n} y_a\, E_a = 0\,, \qquad \sum_{a=1}^{n} \sigma_a\, y_a\, E_a = 0\,, \qquad \sum_{a=1}^{n} y_a^2\, E_a = 0\,. \tag{3.19}$$

JHEP06(2016)101

In order to define local residues in (3.16), one must remove three of the elements of the map $(\sigma_1, \sigma_2, \ldots, \sigma_n) \mapsto (E_1, E_2, \ldots, E_n)$ from $\mathbb{C}^n \mapsto \mathbb{C}^n$. This is welcome as one can use the PSL$(2,\mathbb{C})$ group to fix the location of three σ_a variables. Using the standard Fadeev-Popov procedure one has

$$\mathcal{I} = \frac{1}{2^3}\int_\Gamma \prod_{a\neq i,j,k} d\sigma_a \prod_{b=1}^{n} \frac{(y_b\, dy_b)}{(y_b^2 - \sigma_b^2 + \Lambda^2)} \times \frac{|i,j,k||p,q,r|}{\prod_{d\neq p,q,r} E_d} H(\sigma, y), \tag{3.20}$$

where the Fadeev-Popov determinants are given by

$$|p,q,r| = \frac{1}{\Lambda^2}\begin{vmatrix} y_p & y_p(\sigma_p + y_p) & y_p(\sigma_p - y_p) \\ y_q & y_q(\sigma_q + y_q) & y_q(\sigma_q - y_q) \\ y_r & y_r(\sigma_r + y_r) & y_r(\sigma_r - y_r) \end{vmatrix} = \frac{2\, y_p y_q y_r}{\Lambda^2}\begin{vmatrix} 1 & y_p & \sigma_p \\ 1 & y_q & \sigma_q \\ 1 & y_r & \sigma_r \end{vmatrix}, \tag{3.21}$$

likewise for $|i,j,k|$ and Γ is the integration cycle defined by the solutions of the $2n-3$ equations

$$y_b^2 - \sigma_b^2 + \Lambda^2 = 0, \qquad b = 1, \ldots n, \tag{3.22}$$

$$E_d = 0, \qquad \text{with } d = 1, \ldots n \text{ and } d \neq p, q, r. \tag{3.23}$$

The 2^3 factor appears when the PSL$(2,\mathbb{C})$ symmetry is fixed and the $(\mathbb{Z}_2)^3$ symmetry $(\sigma_i \to -\sigma_i, \sigma_j \to -\sigma_j, \sigma_k \to -\sigma_k)$ is broken.

Note that the values of σ_i, σ_j and σ_k have been fixed but their branches do not, i.e. y_i, y_j and y_k can still take any of the solutions to $y_b^2 - \sigma_b^2 + \Lambda^2 = 0$.

3.1.1 Promoting Λ to variable

In the previous prescription, (3.20), Λ is a constant parameter. In this section we show how to introduce Λ as a variable.

It is straightforward to check that the integral in (3.16) is invariant by the scale transformation

$$(\sigma_a, y_a, \Lambda) \to \rho(\sigma_a, y_a, \Lambda),\ \rho \in \mathbb{C}^* \text{ and } a = 1, \ldots, n, \tag{3.24}$$

Note that the PSL$(2,\mathbb{C})$ measure

$$\frac{d\sigma_i d\sigma_j d\sigma_k}{|i,j,k|}, \tag{3.25}$$

is also invariant by the scale transformation in (3.24).

In order to promote the Λ parameter to a variable we introduce the scale invariant measure $\frac{d\Lambda}{\Lambda}$. Thus, the new measure

$$\frac{d\Lambda}{\Lambda}\frac{d\sigma_i d\sigma_j d\sigma_k}{|i,j,k|}, \tag{3.26}$$

is also scale and PSL$(2,\mathbb{C})$ invariant, i.e GL$(2,\mathbb{C})$ invariant. Clearly, the generators of this GL$(2,\mathbb{C})$ symmetry are given by the elements $\{L_0, L_{-1}, L_1\}$ and the scale generator

$$D = \sum_{a=1}^{n} \sigma_a \partial_a + \Lambda \partial_\Lambda. \tag{3.27}$$

JHEP06(2016)101

Its algebra is given by

$$[L_{\pm 1}, L_0] = \pm L_{\pm 1}, \quad [L_1, L_{-1}] = 2L_0, \quad [D, L_m] = 0, \;\; m \in \{-1, 0, 1\}, \tag{3.28}$$

on the support of the algebraic curve $y_a^2 = \sigma_a^2 - \Lambda^2$.

Now, note that the denominator in (3.25) can be written as the following determinant

$$\Lambda\,|i,j,k| = \frac{1}{\Lambda^2}\begin{vmatrix} y_i & y_i(\sigma_i + y_i) & y_i(\sigma_i - y_i) & \sigma_i \\ y_j & y_j(\sigma_j + y_j) & y_j(\sigma_j - y_j) & \sigma_j \\ y_k & y_k(\sigma_k + y_k) & y_k(\sigma_k - y_k) & \sigma_k \\ 0 & 0 & 0 & \Lambda \end{vmatrix} \equiv \Delta_{\rm FP}(ijk;\Lambda). \tag{3.29}$$

This determinant is just the Fadeev-Popov determinant for the gauge fixing of the three punctures $(\sigma_i, \sigma_j, \sigma_k)$ and the branch cut variable Λ.

Finally, we can rewrite the (3.16) prescription as

$$\mathcal{I} = \frac{1}{\mathrm{Vol}(\mathrm{GL}(2,\mathbb{C}))}\int \frac{d\Lambda}{\Lambda}\int d^n\sigma \prod_{b=1}^{n}\frac{(y_b\, dy_b)}{(y_b^2 - \sigma_b^2 + \Lambda^2)} \times \frac{H(\sigma, y)}{\prod_{d=1}^{n} E_d}. \tag{3.30}$$

Fixing the $\{E_p, E_q, E_r\}$ scattering equations , the $(\sigma_i, \sigma_j, \sigma_k)$ punctures and the Λ branch cut variable one obtains

$$\mathcal{I} = \frac{1}{2^3}\int_\Gamma \prod_{a\neq i,j,k} d\sigma_a \prod_{b=1}^{n}\frac{(y_b\, dy_b)}{(y_b^2 - \sigma_b^2 + \Lambda^2)} \times \frac{\Delta_{\rm FP}(ijk;\Lambda)\;|p,q,r|}{\Lambda} \times \frac{H(\sigma, y)}{\prod_{d\neq p,q,r} E_d}, \tag{3.31}$$

which is the same expression as in (3.20).

3.2 Equivalence with the CHY construction

The idea of this section is to show how the (3.16) prescription is in fact equivalent to the original CHY approach.

Let us define a map from the double-cover version of the sphere into a single cover of $\mathbb{CP}^1$. This should take us back to the original CHY construction. Such a map is very well known and it is given by

$$\sigma_a = \frac{\Lambda}{2}\left(z_a + \frac{1}{z_a}\right), \tag{3.32}$$

where $\Lambda \neq \{0, \infty\}$ is a constant and z_a are the coordinates on $\mathbb{C}P^1$ (CHY coordinates). The first observation is that if all the punctures are located on the same branch, say the upper sheet, i.e. $y_a = +\sqrt{\sigma_a^2 - \Lambda^2}$, then

$$\tau_{a:b} = \frac{1}{2}\left(\frac{y_a + y_b + \sigma_{ab}}{y_a}\right)\frac{1}{\sigma_{ab}} = \left(\frac{2}{\Lambda}\right)\frac{z_a^2}{(z_a^2 - 1)} \times \frac{1}{z_{ab}}. \tag{3.33}$$

In this expression it is easy to see that the lack of antisymmetry in the labels translate into an overall factor in the z_a variables. Also it is simple to show

$$d\sigma_a = \left(\frac{\Lambda}{2}\right)\frac{(z_a^2 - 1)}{z_a^2}\, dz_a, \tag{3.34}$$

JHEP06(2016)101

which means that

$$\frac{1}{2}\left(\frac{y_a+y_b+\sigma_{ab}}{y_a}\right)\frac{d\sigma_a}{\sigma_{ab}}=\frac{dz_a}{z_{ab}}. \tag{3.35}$$

This is indeed the natural differential form on Σ with simple poles at $(\sigma_a, y_a) = (\sigma_b, y_b)$ and at $\sigma_a = \infty$ with residues 1 and -1 respectively.

Therefore, it is straightforward to conclude

$$H(\sigma,y)=\left(\frac{2}{\Lambda}\right)^{2n}\left(\prod_{a=1}^{n}\frac{z_a^2}{z_a^2-1}\right)^2 H(z) \tag{3.36}$$

$$E_a(\sigma,y)=\sum_{i\neq a}^{n}s_{ai}\,\tau_{a:i}=\left(\frac{2}{\Lambda}\right)\left(\frac{z_a^2}{z_a^2-1}\right)\sum_{i\neq a}^{n}\frac{s_{ai}}{z_{ai}}=\left(\frac{2}{\Lambda}\right)\left(\frac{z_a^2}{z_a^2-1}\right)E_a(z), \tag{3.37}$$

where $H(z)$ is as in (3.4).

Carrying out the integration over the y_a variables on the contour given by the solutions $y_a = +\sqrt{\sigma_a^2-\Lambda^2}$ and performing the map (3.32), then (3.16) becomes

$$\begin{aligned}&\frac{1}{\mathrm{Vol}(\mathrm{PSL}(2,\mathbb{C}))}\int\prod_{a=1}^{n}\frac{(y_a\,dy_a)}{(y_a^2-\sigma_a^2+\Lambda^2)}\left(d^n\sigma\,\frac{H(\sigma,y)}{\prod_{b=1}^{n}E_b(\sigma,y)}\right)\Bigg|_{y_a=+\sqrt{\sigma_a^2-\Lambda^2}}\\ &\quad=\left(\frac{1}{2^n}\right)\frac{1}{\mathrm{Vol}(\mathrm{PSL}(2,\mathbb{C}))}\int\prod_{a=1}^{n}dz_a\frac{H(z)}{\prod_{b=1}^{n}E_b(z)},\end{aligned} \tag{3.38}$$

where the $\frac{1}{2^n}$ factor comes from the integral

$$\int\prod_{a=1}^{n}\frac{(y_a\,dy_a)}{(y_a^2-\sigma_a^2+\Lambda^2)}\Bigg|_{y_a=+\sqrt{\sigma_a^2-\Lambda^2}}=\frac{1}{2^n}. \tag{3.39}$$

Computing the integral over all possible configurations, this means the 2^n way of choosing $(y_1 = \pm\sqrt{\sigma_1^2-\Lambda^2}, \ldots, y_n = \pm\sqrt{\sigma_n^2-\Lambda^2})$, and performing the map (3.32), one obtains

$$\begin{aligned}&\frac{1}{\mathrm{Vol}(\mathrm{PSL}(2,\mathbb{C}))}\int\prod_{a=1}^{n}\frac{(y_a\,dy_a)}{(y_a^2-\sigma_a^2+\Lambda^2)}\left(d^n\sigma\,\frac{H(\sigma,y)}{\prod_{b=1}^{n}E_b(\sigma,y)}\right)\\ &\quad=\frac{1}{\mathrm{Vol}(\mathrm{PSL}(2,\mathbb{C}))}\int\prod_{a=1}^{n}dz_a\frac{H(z)}{\prod_{b=1}^{n}E_b(z)}.\end{aligned} \tag{3.40}$$

This result agrees with the original CHY formula.

4 New gauge fixing

In this section we find that by using the full GL(2) redundancy one can gauge fix the location of four punctures, modulo branches. Thus, promoting Λ to a variable to be fixed by the scattering equations, one has the possibility of using a global residue theorem [14] that leads to a new diagrammatic expansion of general amplitudes. Moreover, the residue theorem allows the analytic evaluation of integrals with rational functions whose answers have non-local poles and thus are hard to obtain by other means.

JHEP06(2016)101

4.1 New gauge fixing

Let us start by reviewing the generations of the $\mathrm{GL}(2,\mathbb{C})$ redundancy, as we did in (3.17) in section 3,

$$L_{\pm 1} = \sum_{a=1}^{n} \frac{1}{\Lambda} y_a(\sigma_a \mp y_a)\partial_a, \qquad L_0 = \sum_{a=1}^{n} y_a \partial_a, \qquad D = \sum_{a=1}^{n} \sigma_a \partial_a + \Lambda \partial_\Lambda, \tag{4.1}$$

where $y_a^2 = \sigma_a^2 - \Lambda^2$. Since all four vectors act on σ's one can use them to fix four of the punctures' σ. For simplicity of notation let us assume that they are $\sigma_1, \sigma_2, \sigma_3$ and σ_4. The Fadeev-Popov jacobian, Δ_{FP}, is now

$$\Delta_{\mathrm{FP}}(1234) = \frac{1}{\Lambda^2} \det \begin{pmatrix} y_1 & y_1(\sigma_1 + y_1) & y_1(\sigma_1 - y_1) & \sigma_1 \\ y_2 & y_2(\sigma_2 + y_2) & y_2(\sigma_2 - y_2) & \sigma_2 \\ y_3 & y_3(\sigma_3 + y_3) & y_3(\sigma_3 - y_3) & \sigma_3 \\ y_4 & y_4(\sigma_4 + y_4) & y_4(\sigma_4 - y_4) & \sigma_4 \end{pmatrix}. \tag{4.2}$$

In addition to this one still has to remove three elements from the map $\{E_1, E_2, \ldots, E_n\}$. This procedure is not affected by the new gauge choice and the formula used in (3.20) is still valid. Putting all together and removing, without loss of generality, the scattering equations E_1, E_2 and E_3 we arrive at the new formula

$$\mathcal{I} = \frac{1}{2^3} \int_\Gamma \frac{d\Lambda}{\Lambda} \prod_{a=5}^{n} d\sigma_a \prod_{b=1}^{n} \frac{(y_b\, dy_b)}{(y_b^2 - \sigma_b^2 + \Lambda^2)} \times \frac{\Delta_{\mathrm{FP}}(1234)\,|1,2,3|}{\prod_{d=4}^{n} E_d} H(\sigma, y), \tag{4.3}$$

where Γ is the integration cycle defines as in (3.22), given by the equations

$$\begin{aligned} y_b^2 - \sigma_b^2 + \Lambda^2 = 0, \qquad & b = 1, \ldots n, \\ E_d = 0, \qquad & \text{with } d = 4, \ldots n, \end{aligned} \tag{4.4}$$

for the $2n-3$ variables $(\Lambda, \sigma_5, \ldots, \sigma_n, y_1, y_2, \ldots, y_n)$.

It is interesting to note that the opening of the branch cut connecting the two branches (sheets) becomes a function of the kinematic invariants $k_a \cdot k_b$. This means that as we move in the space of kinematic invariants the branch cut also moves. This is what makes factorization and crossing natural properties to address using this formulation.

5 Residue theorem and diagrammatic expansion

The equations obtained at the end of the previous section are polynomial equations of increasing degree as the number of particles increases. In fact, the equations (4.4) lead to higher degree polynomials than the original CHY scattering equations. This seems to be an obstacle. However, using a residue theorem we will effectively replace one of the $E_a = 0$ equations by the equation $\Lambda = 0$. This might come as a surprise as closing the cut is intuitively related to a factorization limit. Instead, what we will see is that once the cut closes a new puncture appears that represents an off-shell particle. The sum over solutions to the equations $y_b^2 = \sigma_b^2 - \Lambda^2$ give rise to $y_b = \pm\sigma_b$ and determine the branch

JHEP06(2016)101

location of the b^{th}-puncture. For a given distribution of particles, say a subset U (L) is on the upper (lower) branch, the equation E_a that was eliminated gives rise to the propagator $1/P_U^2$ where P_U is the sum over the momenta of all external particles on the upper branch. In this way, the integral given in (4.3)

$$\mathcal{I} = \frac{1}{2^3}\int_\Gamma \frac{d\Lambda}{\Lambda}\prod_{a=5}^{n} d\sigma_a \prod_{b=1}^{n}\frac{(y_b\, dy_b)}{(y_b^2-\sigma_b^2+\Lambda^2)} \times \frac{\Delta_{\text{FP}}(1234)\ |1,2,3|}{\prod_{d=4}^{n} E_d(\sigma,y)} H(\sigma,y) \tag{5.1}$$

becomes a sum of products of contour integrals with smaller number of particles. By iterating the process we find a diagrammatic description. The most important outcome is that at each step in the iteration process the degree of the scattering equation is lowered and analytic evaluations become possible.

5.1 Residue theorem

Following the similar ideas as in section 3.2 les us consider the general integral

$$\mathcal{I} = \frac{1}{\text{Vol}(\text{GL}(2,\mathbb{C}))}\int_\gamma d\Lambda \left(\prod_{b=1}^{n}\frac{dy_b}{(y_b^2-\sigma_b^2+\Lambda^2)}\right)\left(\prod_{a=1}^{n}\frac{d\sigma_a}{\tilde{E}_a(\sigma,y)}\right)\frac{H(\sigma,y)\prod_{c=1}^{n} y_c^2}{\Lambda}, \tag{5.2}$$

where γ is the contour defined by the equations

$$y_a^2-\sigma_a^2+\Lambda^2=0, \quad \tilde{E}_a(\sigma,y)=\sum_{b\neq a}\frac{k_a\cdot k_b}{\sigma_{ab}}(y_b+y_a)=0, \quad \text{for} \quad a\in\{1,2,\ldots,n\}, \tag{5.3}$$

and $H(\sigma,y)\prod_{c=1}^{n} y_c^2/\Lambda$ is the integrand. Clearly there are more integration variables than contours, nevertheless, when the $\text{GL}(2,\mathbb{C})$ symmetry is fixed then the number of integration variables becomes equal to the contour cycles.

Note that (5.2) depends over the Λ variable by the expression

$$\int \frac{d\Lambda}{\prod_{b=1}^{n}(y_b^2-\sigma_b^2+\Lambda^2)}\times\frac{1}{\Lambda}, \tag{5.4}$$

where $\prod_{b=1}^{n}(y_b^2-\sigma_b^2+\Lambda^2)$ defines the integration cycle. Naively, using the global residue theorem, it is straightforward to see that the previous expression can be written as

$$\int \frac{d\Lambda}{\prod_{b=1}^{n}(y_b^2-\sigma_b^2+\Lambda^2)}\times\frac{1}{\Lambda} = -\int \frac{d\Lambda}{\Lambda\ \prod_{b\neq l}^{n}(y_b^2-\sigma_b^2+\Lambda^2)}\times\frac{1}{y_l^2-\sigma_l^2+\Lambda^2}, \tag{5.5}$$

where $\Lambda\ \prod_{b\neq l}^{n}(y_b^2-\sigma_b^2+\Lambda^2)$ defines the new contour and $1/(y_l^2-\sigma_l^2+\Lambda^2)$ becomes part of the integrand.

Nevertheless, in order to apply the global residue theorem one must also verify if the point at infinity is a pole. One says that the (5.2) integral has a pole at infinity if and only if [14]

$$\deg(g) > (d_1+\cdots+d_{2n})-((2n+1)+1), \tag{5.6}$$

where $g(\sigma,y,\Lambda)$ is the integrand

$$g(\sigma,y,\Lambda)=\frac{H(\sigma,y)\prod_{c=1}^{n} y_c^2}{\Lambda} \quad\Rightarrow\quad \deg(g)=-1, \tag{5.7}$$

JHEP06(2016)101

$d_1+\cdots+d_{2n}$ is sum over all degrees of the polynomials that define the integration contour, i.e.

$$d_1+\cdots+d_{2n}=\deg\left(\prod_{b=1}^{n}(y_b^2-\sigma_b^2+\Lambda^2)\,\tilde{E}_b\right)=2n \tag{5.8}$$

and $2n+1$ is the number of integration variables, i.e. $(\Lambda,\sigma_1,\ldots,\sigma_n,y_1,\ldots,y_n)$. Clearly (5.2) has a pole at infinity and it must be integrated when the global residue theorem is performed.

Since the integrand in (5.2) is not well defined when $\Lambda=0$, then this implies that the (5.2) integrand is given on the $\Lambda\neq 0$ chart . Thus, so as to explore the pole at infinity we consider the following transformation

$$\Lambda\;\to\;\Lambda'=\frac{1}{\Lambda},\quad y_i\;\to\;y_i'=\frac{y_i}{\Lambda^2},\quad \sigma_i\;\to\;\sigma_i'=\frac{\sigma_i}{\Lambda^2}. \tag{5.9}$$

Under this transformation (5.2) becomes invariant, i.e.

$$\mathcal{I}=\frac{1}{\mathrm{Vol}(\mathrm{GL}(2,\mathbb{C}))}\int_{\gamma'}d\Lambda'\left(\prod_{b=1}^{n}\frac{dy_b'}{({y_b'}^2-{\sigma_b'}^2+{\Lambda'}^2)}\right)\left(\prod_{a=1}^{n}\frac{d\sigma_a'}{\tilde{E}_a(\sigma',y')}\right)\frac{H(\sigma',y')\prod_{c=1}^{n}{y_c'}^2}{\Lambda'}, \tag{5.10}$$

where γ' is the contour defined by the equations

$${y_a'}^2-{\sigma_a'}^2+{\Lambda'}^2=0,\quad \tilde{E}_a(\sigma',y')=\sum_{b\neq a}^{n}\frac{k_a\cdot k_b}{\sigma_{ab}'}(y_a'+y_b')=0, \tag{5.11}$$

and $H(\sigma',y')$ is defined with the $\tau_{a:b}'$'s forms

$$\tau_{ab}'=\frac{1}{2\,y_a'}\left(\frac{y_a'+y_b'+\sigma_{ab}'}{\sigma_{ab}'}\right). \tag{5.12}$$

Note that the minus sign $d\Lambda/\Lambda\to -d\Lambda'/\Lambda'$ is used to reorient the Λ contour. Finally, we can now integrate around the point $\Lambda'=0$ which is the pole at infinity, therefore performing the global residue theorem the (5.2) integral could be read as

$$\mathcal{I}=\frac{-2}{\mathrm{Vol}(\mathrm{GL}(2,\mathbb{C}))}\int_{\tilde{\Gamma}}\frac{d\Lambda}{\Lambda}\left(\frac{\prod_{i=1}^{n}dy_i}{\prod_{b\neq l}^{n}(y_b^2-\sigma_b^2+\Lambda^2)}\right)\left(\prod_{a=1}^{n}\frac{d\sigma_a}{\tilde{E}_a(\sigma,y)}\right)\frac{H(\sigma,y)\prod_{c=1}^{n}y_c^2}{(y_l^2-\sigma_l^2+\Lambda^2)}, \tag{5.13}$$

where the new $\tilde{\Gamma}$ contour is now defined by the $2n$ equations

$$\Lambda=0,\quad y_b^2-\sigma_b^2+\Lambda^2=0,\quad \text{for}\quad b\neq l,\quad \tilde{E}_a(\sigma,y)=0,\quad \text{for}\quad a\in\{1,2,\ldots,n\}. \tag{5.14}$$

5.2 Recovering the curve

Note that in the result obtained in (5.13) the $y_l^2-\sigma_l^2+\Lambda^2=0$ constraint is lost, i.e. we are not anymore on the support of the curve $y_l^2=\sigma_l^2-\Lambda^2$. Since our aim is to be on a sphere then this constraint must be recovered. In order to get back the $y_l^2-\sigma_l^2+\Lambda^2=0$ equation we perform the residue theorem but now using the y_l variable.

JHEP06(2016)101

Before applying the residue theorem it is useful to remember the following, first, in full view, the integration contour is defined by polynomials over the y_i's variables

$$\Lambda\prod_{b\neq l}^{n}(y_b^2-\sigma_b^2+\Lambda^2))\prod_{a=1}^{n}\tilde{E}_a(\sigma,y)=\Lambda\prod_{b\neq l}^{n}(y_b^2-\sigma_b^2+\Lambda^2))\prod_{a=1}^{n}\left[\sum_{i\neq a}^{n}s_{ab}\left(\frac{y_a+y_i}{\sigma_{ai}}\right)\right],$$

and secondly, the integrand

$$\frac{H(\sigma,y)\prod_{c=1}^{n}y_c^2}{(y_l^2-\sigma_l^2+\Lambda^2)},$$

has just one singularity over the y_i's variables given by $(y_l^2-\sigma_l^2+\Lambda^2)$. With this in mind, we are ready to use the residue theorem over y_l. The integral by the y_l variable is read as

$$\int_{\tilde{\Gamma}}\frac{dy_l}{\prod_{a=1}^{n}\tilde{E}_a}\times\frac{H(\sigma,y)\prod_{c=1}^{n}y_c^2}{(y_l^2-\sigma_l^2+\Lambda^2)},\tag{5.15}$$

so, performing the residue theorem one obtains[1]

$$\int_{\tilde{\Gamma}}\frac{dy_l}{\prod_{a=1}^{n}\tilde{E}_a}\times\frac{H(\sigma,y)\prod_{c=1}^{n}y_c^2}{(y_l^2-\sigma_l^2+\Lambda^2)}=-\int_{\Gamma}\frac{dy_l}{(y_l^2-\sigma_l^2+\Lambda^2)\prod_{a\neq l}^{n}\tilde{E}_a}\times\frac{H(\sigma,y)\prod_{c=1}^{n}y_c^2}{\tilde{E}_l},\tag{5.16}$$

where Γ is the new integration contour defined by the $2n$ equations

$$\Lambda=0,\quad \tilde{E}_b(\sigma,y)=0,\quad \text{for}\quad b\neq l,\quad y_a^2-\sigma_a^2+\Lambda^2=0,\quad \text{for}\quad a\in\{1,2,\ldots,n\}.\tag{5.17}$$

Finally, the (5.2) integral is written as

$$\mathcal{I}=\frac{2}{\mathrm{Vol}(\mathrm{GL}(2,\mathbb{C}))}\int_{\Gamma}\frac{d\Lambda}{\Lambda}\left(\prod_{b=1}^{n}\frac{dy_b}{(y_b^2-\sigma_b^2+\Lambda^2)}\right)\left(\frac{\prod_{a=1}^{n}d\sigma_a}{\prod_{i\neq l}^{n}\tilde{E}_i(\sigma,y)}\right)\frac{H(\sigma,y)\prod_{c=1}^{n}y_c^2}{\tilde{E}_l}.\tag{5.18}$$

Fixing the $(\sigma_m,\sigma_n,\sigma_p,\sigma_q)$ puctures and the (E_m,E_n,E_q) scattering equations the above integral becomes

$$\mathcal{I}=\frac{1}{2^2}\int_{\gamma}\left(\frac{d\Lambda}{\Lambda}\right)\left(\prod_{b=1}^{n}\frac{(y_b\ dy_b)}{(y_b^2-\sigma_b^2+\Lambda^2)}\right)\left(\prod_{a\neq m,n,p,q}\frac{d\sigma_a}{E_a(\sigma,y)}\right)\frac{|m,n,q|\Delta_{\mathrm{FP}}(mnq,p)H(\sigma,y)}{E_p},\tag{5.19}$$

where the contour γ is defined by the equations

$$\Lambda=0,\quad \tilde{E}_b(\sigma,y)=0,\quad \text{for}\quad b\neq\{m,n,p,q\},\quad y_a^2-\sigma_a^2+\Lambda^2=0,\quad \text{for}\quad a=1,2,\ldots,n.\tag{5.20}$$

We call this integral the Λ-*prescription*.

Note that we have chosen the same labels for the punctures and scattering equations, this will be useful when we will formulate the $\Lambda-$algorithm in section 6.2.

The $\Lambda-$prescription, (5.19), recovered the support on the curves $y_a^2=\sigma_a^2-\Lambda^2$, moreover, it must be computed around the cycles $\Lambda\to 0$ and $\Lambda\to\infty$, which are exactly the same, as one can see in figure 1.

[1]There is no contribution from the point at infinity.

JHEP06(2016)101

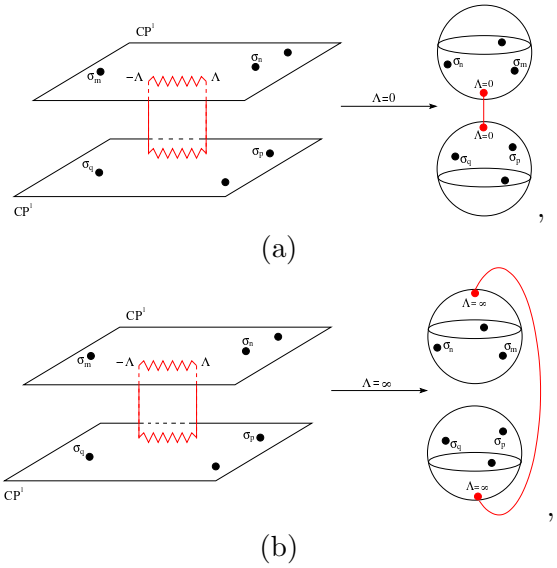

Figure 1. (a) Limit $\Lambda \to 0$. (b) Limit $\Lambda \to \infty$.

In addition, one of the $(n-3)$ scattering equations becomes free, i.e. it now is part of the integrand, in (5.19) it is E_p.

This new point of view gives us a new kind of diagrammatic representation, figure 1. In the next section we will learn to use this new prescription and we will propose a new algorithm (the $\Lambda-$algorithm).

6 Λ-diagrams and a new algorithm

Here we present a new algorithm, which is a consequence of the new prescription given in (5.19).

Before formulating the algorithm we introduce some notations. Let us remember the $s_{a_1\dots a_n}$ Mandelstam variables are defined as[2]

$$s_{a_1\dots a_n} := \frac{1}{2}(k_{a_1} + \cdots + k_{a_n})^2. \tag{6.1}$$

Nevertheless, it will be useful for us to use the variables

$$k_{a_1\dots a_n} := \sum_{a_i<a_j}^{n} k_{a_i} \cdot k_{a_j}, \tag{6.2}$$

Clearly, when the particles are massless, i.e. $k_i^2 = 0$, then $s_{a_1\dots a_n} = k_{a_1\dots a_n}$.

In the next two section, 6.1 and 6.1.1, we give all tools to formulate our new algorithm in section 6.2. While we develope the sections 6.1 and 6.1.1, we apply all these tools on a simple and particular example and at the end we obtain the result for the (5.19) integral.

[2]We have introduced the (1/2) factor for convenience.

JHEP06(2016)101

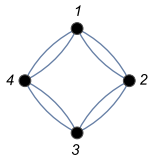

Figure 2. G graph associated to the integrand in (6.4).

6.1 More notations and a simple example

In the same way as in [17], any $H(\sigma, y)$ integrand over $\mathcal{M}_{0,n}$ can be written as a linear combinations of integrands with no zeros , i.e. integrands with just $2n - \tau_{a:b}$ factors. We call this kind of integrands as[3] $H^D(\sigma)$. Each $H^D(\sigma)$ integrand has associated a 4-regular graph[4] (bijective map), which we denoted by $G = (V_G, E_G)$ [17, 58, 59]. The vertex set of G is given by the n-labels (punctures)

$$V_G = \{1, 2, \ldots, n\}$$

and the edge set is given by the elements $\tau_{a:b} \leftrightarrow \overline{a\, b}$, i.e.

$$E_G = \{\ \overline{a\, b}\ /\ \tau_{a:b}\ \text{ is a factor into the }\ H^D(\sigma)\quad \text{integrand. }\}.$$

Since $\tau_{a:b}$ always appears into a chain, for instance, let us remember the smallest chain is given by

$$\tau_{a:b}\tau_{b:a}, \tag{6.3}$$

then the graph is not a directed graph, as well as in [17].

For example, let us consider the integrand

$$H_4^D(1, 2, 3, 4) = [1234] \times [1234]\,, \tag{6.4}$$

where the $[\,\cdot\,]$ bracket is defined as

$$[1234] = (\tau_{1:2}\tau_{2:3}\tau_{3:4}\tau_{4:1})\ . \tag{6.5}$$

This integrand is represented by the G graph in figure 2.

This is useful to clarify that the G graph must be draw such that the number of intersection among the edges is as small as possible.

Note that the G graph does not have any information of the $\mathrm{GL}(2, \mathbb{C})$ symmetry and the Λ parameter or branch cut. In order to introduce this information on the graph we coloured the vertex set in the way given in figure 3.

The G graph can now contain the whole information of the integrand, i.e, it now represents the total integrand $\mathcal{I} = |ijk|\Delta_{FP}(ijk, d)H(\sigma)$.

For example, using the $\mathrm{PSL}(2, \mathbb{C})$ symmetry to fix the $(\sigma_1, \sigma_2, \sigma_3)$ punctures and the scale symmetry to fix the σ_4 puncture, the graph in figure 2 becomes as in figure 4, where figure 4(c) shows the whole possibles non-zero contributions or configurations, up to $\mathbb{Z}_2$ symmetry $y_a \to -y_a$, after performing the Λ integral around $\Lambda = 0$. It is explained in detail in the next section.

[3]The D letter means that there are only σ_a factors into denominator.

[4]A G graph is defined by the two finite sets, V and E. V is the vertex set and E is the edge set.

JHEP06(2016)101

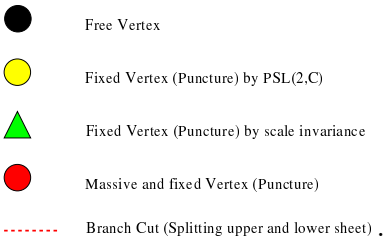

Figure 3. Coloured Vertices.

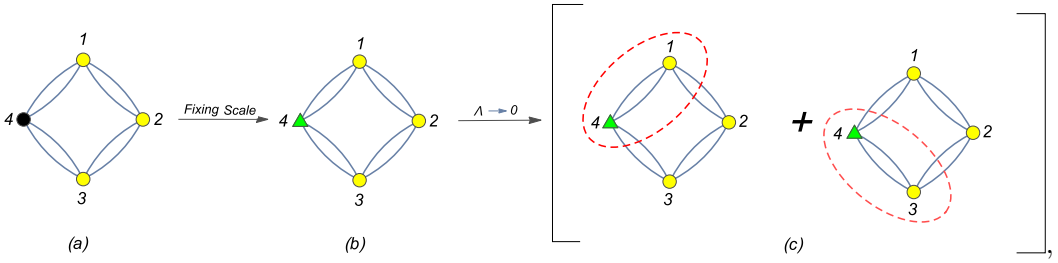

Figure 4. (a) Fixing $(\sigma_1, \sigma_2, \sigma_3)$ from the PSL$(2, \mathbb{C})$ symmetry. (b) Fixing σ_4 from the scale symmetry. (c) Possibles contribution after performing the Λ integral.

6.1.1 Configurations and Λ-theorem

Although we previously have already used the word "*configuration*", in this section we give a formal definition. So, the first thing we do in this section is to define what is a configuration

- **Configuration:** a configuration, which we denoted by C, is the integration over the $(y_1, \dots y_n)$ variables around one of the 2^n solutions of the equations

$$y_a^2 - \sigma_a^2 + \Lambda^2 = 0, \quad \text{for } a = 1 \dots n. \tag{6.6}$$

This definition means that a C configuration is the choosing of the 2^n possibilities given by $(y_1 = \pm\sqrt{\sigma_1^2 - \Lambda^2}, \dots, y_n = \pm\sqrt{\sigma_n^2 - \Lambda^2})$, i.e. a configuration fixed the punctures on the upper or lower sheet.

Now, with this in mind we are ready to come back to our example and note that besides of two configurations given in figure 4(c), there are more possibles configurations (up to $\mathbb{Z}_2$ symmetry) such as

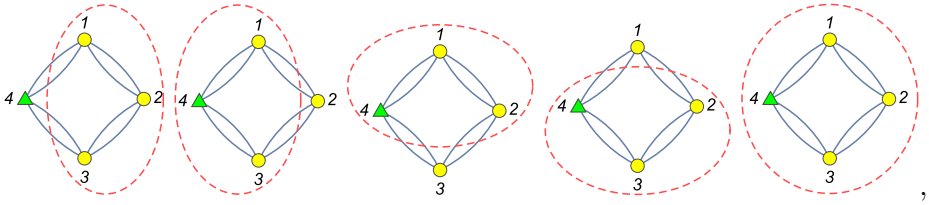

where the red line enclose the punctures on the same branch cut, i.e. the red line is the branch cut, which is controled by the Λ integration variable.

JHEP06(2016)101

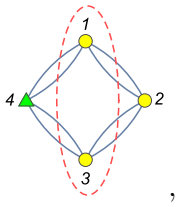

Figure 5. Allowable configuration which vanishes.

However, these five configurations vanish trivially because the PSL$(2,\mathbb{C})$ symmetry is breaking on upper and lower sheet when $\Lambda \to 0$. This computation is straightforward.

So as to classify the different kind of configurations we introduce the following terminology

- **Allowable configuration:** let C be a configuration. We say C is an *allowable configuration* if the number of fixed punctures on the upper and lower sheet is two. This implies that in the $\Lambda \to 0$ limit the PSL$(2,\mathbb{C})$ symmetry is well defined (gauged) on each sheet.

Clearly, for the diagram in figure 4 there is one more *allowable configuration* given in figure 5, but this one also vanishes.

The vanishing of this last configuration is a consequence of the following theorem

Λ-theorem. Let C be an allowable configuration, then the integrand $\mathcal{I} = |ijk|\Delta_{FP}(ijk,d)H^D(\sigma)$ on the C configuration has the $\Lambda-$behavior

$$\mathcal{I}\Big|^{C}_{\Lambda\to 0} \sim \Lambda^{L-4} + \mathcal{O}(\Lambda^{L-3})$$

around $\Lambda = 0$, where L is the number of edges which are intersected by the red line.

This theorem is proved in appendix A.

So far, we have defined what is a configuration, an allowable configuration and we have formulated the $\Lambda-$theorem. Now, with the intention to set down the $\Lambda-$algorithm it is useful to define a new kind of configuration

- **Singular configuration:** let C be a configuration. We say C is an *singular configuration* if C is an allowable configuration and the integrand, $\mathcal{I} = |ijk|\Delta_{FP}(ijk,d)H(\sigma) \sim \Lambda^{-s}$, $s > 0$ around $\Lambda = 0$.

Following with our example, we note that expanding the $\mathcal{I} = |123|\Delta_{FP}(123,4)H_4^D(1,2,3,4)$ total integrand and the E_4 scattering equation (S.E) around $\Lambda = 0$, the two configurations in figure 4(c) become as in figure 6. Thus, the integration over Λ is straightforward and the final result is given in figure 7, which is the right answer.

We call this method the $\Lambda-$algorithm. In the next section we explain carefully this algorithm.

JHEP06(2016)101

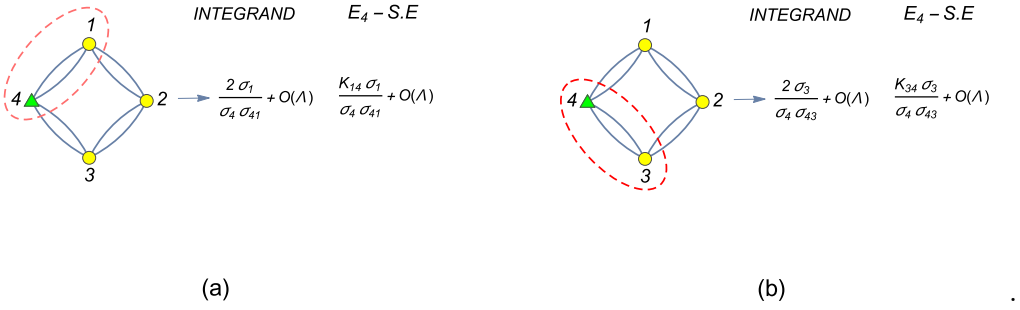

Figure 6. Computing the non-zero allowable configurations.

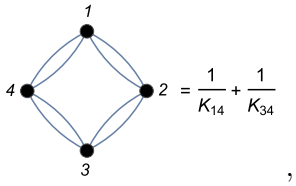

Figure 7. Final solution for the integrand in (6.4).

6.2 The Λ-algorithm

In this section we introduce formally the $\Lambda-$algorithm, which is given up to $\mathbb{Z}_2$ symmetry,, $y_a \rightarrow -y_a$.

We describe step by step the method.

Λ-algorithm steps.

- **(1)** To draw the graph to be computed. Let us remember that the graph must be drawn such that the intersection number of the edges is the minimum.

  This drawing must have three yellow vertices (PSL$(2,\mathbb{C})$ gauge fixing) and one green vertex (scale symmetry fixing)

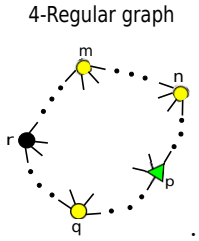

Figure (a). 4-Regular graph. PSL$(2,\mathbb{C})$ (Yellow) and scale symmetry (Green) gauge fixing.

- **(2)** To find all non-zero allowable configurations

JHEP06(2016)101

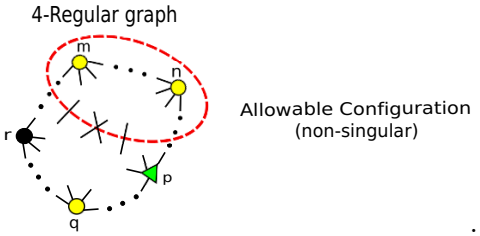

Figure (b). One non-zero allowable configuration.

The gauge fixing from the step (1) must be chosen such that there are not singular configurations. This fact becomes clearer in section 7.

If it is not possible to choose a gauge fixing such that it avoids singular configurations then the $\Lambda-$algorithm can not be applied directly.

From the $\Lambda-$theorem, it is clear that the red line in all non zero configurations intersects only 4 black lines, i.e. just 4 black lines go through the branch cut.

- **(3)** To compute the Λ integral around the cycle $|\Lambda| = \epsilon$ (on all configurations found in the previous step).

  - **(i)** After computing the Λ integral (on one particular configuration) the sphere is splitting into two spheres, the upper-sheet and the lower-sheet. This splitting is identified by the red line. As a consequence two new (massive) punctures arise, one on the upper and the other one on the lower-sheet. These punctures are fixed on each sheet at the point $\sigma_0 = 0$ and they are denoted by the red color. This process is shown in the following figure

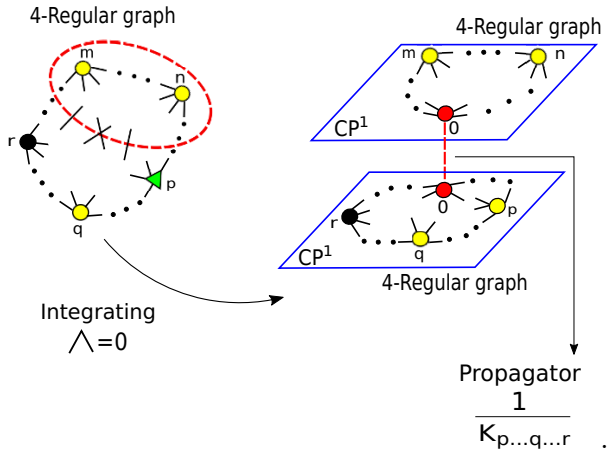

Figure (c). Computating the Λ integral on one particular configuration.

The particles inside of the red line, including now the new red massive puncture at $\sigma_0 = 0$ on the upper-sheet, shape a new 4-regular graph on the upper-sheet (subdiagram) and the particles outside of the red line, including the new red massive puncture at $\sigma_0 = 0$ on the lower-sheet, shape the other new 4-regular graph (subdiagram), such as it is shown in figure (c).

JHEP06(2016)101

The momentum of the red massive puncture on the upper-sheet is the sum over all momenta of the particles outside of the red line, i.e.

$$k_0^{\text{upper}} = k_p + \cdots + k_q + \cdots + k_r + \cdots , \tag{6.7}$$

and the momentum of the red massive puncture on the lower-sheet is the sum over all momenta of the particles inside of the red line, i.e.

$$k_0^{\text{lower}} = k_m + \cdots + k_n + \cdots . \tag{6.8}$$

– **(ii)** The scattering equation associates to the puncture in the green triangle, in figure (c) it is E_p, becomes.

$$E_p = \sum_{a \neq \text{upper sheet}} \frac{k_p \cdot k_a}{\sigma_{pa}} + \frac{k_p \cdot k_0^{\text{lower}}}{\sigma_p} + \mathcal{O}(\Lambda).$$

Using the scattering equations (at $\Lambda = 0$) located on the same sheet as the green puncture, in figure(c) it is the lower sheet, i.e $E_r, \ldots$, it is straightforward to prove that

$$E_p = -\frac{(\sigma_q - \sigma_0)(\sigma_0 - \sigma_q)}{(\sigma_0 - \sigma_p)(\sigma_p - \sigma_q)(\sigma_q - \sigma_0)} k_{p\ldots q\ldots r\ldots} + \mathcal{O}(\Lambda) ,$$

where $\sigma_0 = 0$. The $(\sigma_0 - \sigma_p)(\sigma_p - \sigma_q)(\sigma_q - \sigma_0)$ factor becomes one of the two Faddeev-Popov determinants on the lower brach and the numerator, $(\sigma_q - \sigma_0)(\sigma_0 - \sigma_q)$, cancels out with the $|m, n, q|\, \Delta_{\text{FP}}(mnq, p)$ Faddeev-Popov expansion given in appendix A. Therefore, one can say that the E_p scattering amplitude becomes the propagator

$$\frac{1}{E_p} \quad \rightarrow \quad \frac{1}{k_{p\ldots q\ldots r\ldots}} .$$

Note that although in our example (figure (c)) $k_{p\ldots q\ldots r\ldots} = k_{m\ldots n\ldots}$, in general this is not true. Since the $\Lambda-$algorithm is a iterative process then new massive particles arise (red punctures) and the equality $k_{p\ldots q\ldots r\ldots} = k_{m\ldots n\ldots}$ can be broken. Finally, the two new subdiagrams are given in the original CHY approach, where $(\sigma_0, \sigma_m, \sigma_n)$ are the gauged punctures on the upper-sheet and $(\sigma_0, \sigma_p, \sigma_q)$ are the gauged punctures on the lower-sheet.

- **(4)** To come back to the step (1).

It is useful to remember that a 4-regular graph with 3 vertices is just 1

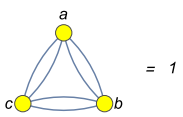

Figure (d). 3-point 4-regular graph.

JHEP06(2016)101

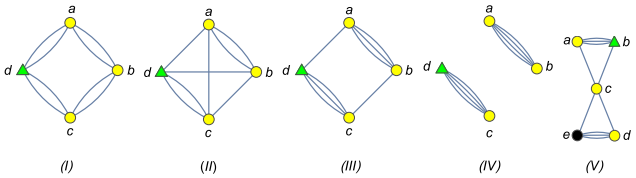

Figure 8. Building Blocks.

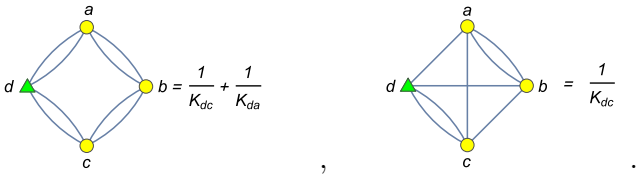

Figure 9. Building Blocks (I) and (II).

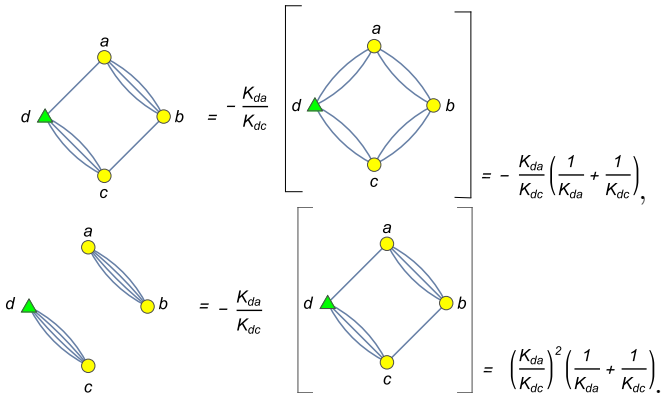

Figure 10. Building Blocks (III) and (IV).

6.3 Building blocks

Since that the Λ-algorithm is an iterative process then it is useful to construct fundamental graphs or irreducible graphs (building blocks).

Our building blocks are given by the following diagrams of 4 and 5 vertices in figure 8. The (I) graph, which was computed previously, and (II) graph are trivials and their results are given in figure 9 [2].

In order to compute the the (II) and (III) building blocks, one can note that on the support of the E_d scattering equation (before performing the residue theorem, section 5)

$$E_d = k_{ad}\,\tau_{d:a} + k_{bd}\,\tau_{d:b} + k_{cd}\,\tau_{d:c} = 0 \;\Rightarrow\; -1 = \frac{k_{ad}}{k_{cd}}\left(\frac{\tau_{d:a}\tau_{b:c}}{\tau_{b:a}\tau_{d:c}}\right) . \tag{6.9}$$

So, the (III) and (IV) graphs in figure 8 become very simples, see figure 10.

Finally, the (V) building block in figure 8 can not be computed using the $\Lambda-$algorithm, because this graph has a singular configuration. So, we use the algorithm given in [17] (the general KLT algorithm).

JHEP06(2016)101

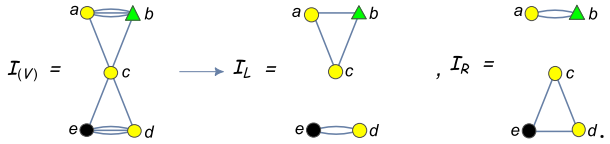

Figure 11. Decomposition in two 2-regular graphs.

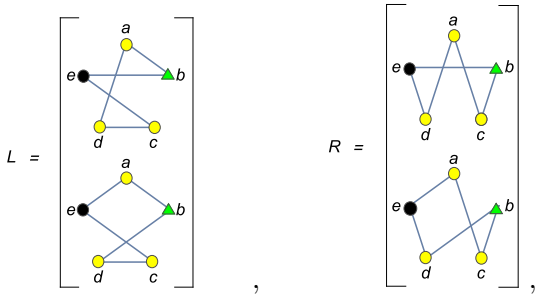

Figure 12. Left and right base.

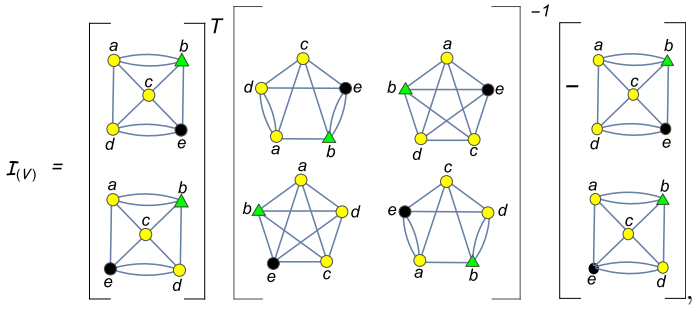

Figure 13. Graph representation of the $\mathcal{I}_{(V)} = (L\mathcal{I}_{\mathcal{L}})^{\mathrm{T}}(m^{L|R})^{-1}(R\mathcal{I}_{\mathcal{R}})$ computation.

6.3.1 General KLT algorithm and computation of the (V) building block

In order to apply the general KLT algorithm [17] on the (V) building block, one must first note that this building block has the following decomposition (in two 2-regular graphs) given in figure 11. The second step is to find a left and right (Parke-Taylor) base *compatible*[5] with the the $\mathcal{I}_{\mathcal{L}}$ and $\mathcal{I}_{\mathcal{R}}$ graphs. Choosing the left and right base as in figure 12, and following the general KLT algorithm [17], it is straightforward to read the (V) building block as in figure 13, where the relative sign was explained in [2].

So as to be consistent with the initial gauge fixing we must keep it,[6] i.e. the color of the vertices.

Although in [2] was given an algorithm to computed the diagrams found in figure 13, we apply the $\Lambda-$algorithm since it works when one of the particles is off-shell.

[5]A Parke-Taylor factor is said to be compatible with a 2-regular graph if the union of the two graphs, which is a 4-regular graph, admits a Hamiltonian decomposition, i.e., it is the union of two Parke-Taylor factors.

[6]This fact is very important, because when the $\Lambda-$algorithm is iterated then massive particles arise and the gauge fixing must be kept step by step to obtain the right answer.

JHEP06(2016)101

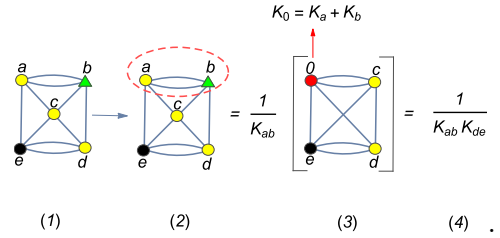

Figure 14. Λ−algorithm. (1) Integrand. (2) Allowable configurations non zero. (3) Computing the Λ integral. (4) Final answer.

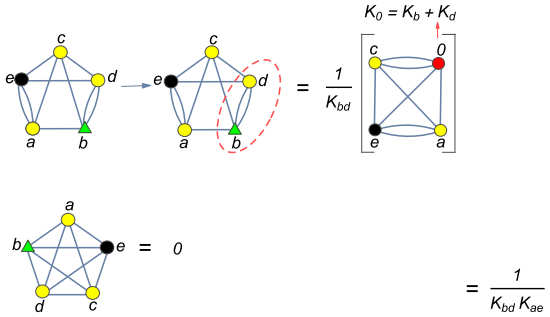

Figure 15. Computation of the $m_{22}^{L|R}$ and $m_{21}^{L|R}$ matrix components, respectively.

Let us consider the second component of the first vector given in figure 13 (see figure 14). In figure 14 we describe step by step the Λ−algorithm for a particular diagram in figure 13:

- **(1)** We draw the graph to be computed, including the gauge fixing (colored vertices).
- **(2)** We find the all non-zero allowable configurations, which is only one.
- **(3)** We compute the Λ integral around $\Lambda = 0$.
  - **(i)** The scattering equation $1/E_b$ becomes the propagator $1/k_{ab}$.
  - **(ii)** The subdiagram obtained on the upper-sheet is a 4-regular graph at three point, which is trivial,, i.e. 1. On the other hand, the 4-regular subdigram obtains on the lower-sheet is a 4-point graph, which is the (II) building block given in figure 8.
  - **(iii)** The new massive particle in the graph on the lower-sheet has momentum $k_0 = k_a + k_b$.
- **(4)** we used the (II) building block in figure 8 to obtain the final answer.

Following the same simple procedure one can compute all graphs in figure 13, for example, the $m_{22}^{L|R}$ and $m_{12}^{L|R}$ matrix components, respectively, are given in figure 15. Therefore, the $\mathcal{I}_{(V)}$ building block is

JHEP06(2016)101

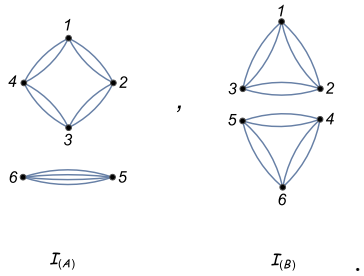

Figure 16. Six-point examples.

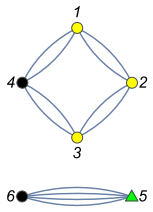

Figure 17. Gauge Fixing.

$$\begin{aligned}\mathcal{I}_{(V)} &= \left(\frac{1}{k_{ab}k_{de}}\right)^2 \begin{pmatrix}1\\1\end{pmatrix}^{\mathrm{T}} \begin{pmatrix}\frac{1}{k_{bce}k_{be}} & 0\\ 0 & \frac{1}{k_{ae}k_{bd}}\end{pmatrix}^{-1} \begin{pmatrix}-1\\1\end{pmatrix} \\ &= \left(\frac{1}{k_{ab}k_{de}}\right)^2 (k_{ae}k_{bd} - k_{bce}k_{be}) \ . \end{aligned} \tag{6.10}$$

7 Examples

Although in the previous section we have already applied the $\Lambda-$algorithm, the idea here is to give some non-trivial examples in order to show the power of this new algorithm.

This section is divided as follows, the first example show us how to use the Λ algorithm, which will be applied over a six point highly non trivial diagram. The idea of the second one is to mix the Λ algorithm with the KLT general algorithm [17], where we will compute a six point diagram which cannot be performed just with the Λ algorithm. Finally, the last one is given in order to illustrate the using of all building blocks, with this in mind we choose a non trivial eight point diagram.

7.1 Six-point

Let us consider the following two non-trivial six-point examples in figure 16.

The first one, $\mathcal{I}_{(\mathcal{A})}$, will be computed just using the $\Lambda-$algorithm. For the second one, $\mathcal{I}_{(\mathcal{B})}$, the $\Lambda-$algorithm is not enough. We will combine the Λ and the general KLT algorithm [17] to compute it.

7.1.1 $\mathcal{I}_{(\mathcal{A})}$-computation

In order to avoid singular configurations we choose the gauge fixing given in figure 17.

JHEP06(2016)101

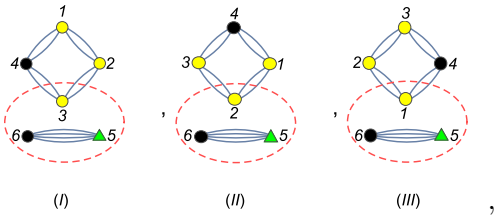

Figure 18. Allowable configurations of type 1.

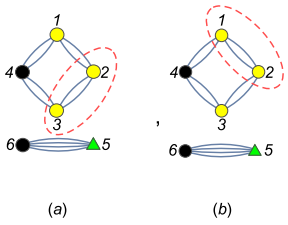

Figure 19. Allowable configurations of type 2.

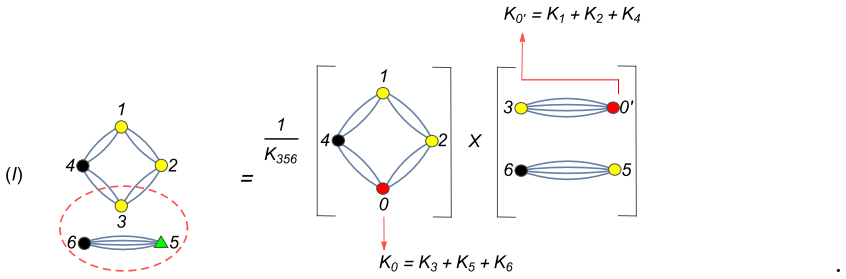

Figure 20. Computing the (I) diagram.

This is straightforward to see that there are two kind of allowable configurations. The first one is given by the diagrams in figure 18 and the second one in figure 19.

Since the elements of each type are totally analogues then we only compute one of each set.

Let us begin by computing the (I) configuration in figure 18. Applying the $\Lambda-$algorithm, the E_5 scattering equation becomes the $1/k_{356}$ propagator and the diagram breaks into two graphs (upper and lower sheet) in the original CHY approach, as it is shown in figure 20. Using the building blocks given in section 6.3 (see figure 9 and figure 10), we are able to find the final answer for the (I) configuration in figure 18. Thus, following the same procedure for the (II) and (III) configurations one obtains the results given in figure 21.

We must now compute the (a) and (b) configurations in figure 19. Let us start with the (a) configuration. From the $\Lambda-$algorithm one has the 5-point subgraph given in figure 22. So as to apply the $\Lambda-$algorithm on the resulting 5-point graph, we must fix the scale symmetry (S.S). We gauge the σ_4 puncture as in figure 23. It is simple to see that the non-zero allowable configurations in figure 23 are given in figure 24. These three configurations are straightforward to compute applying the $\Lambda-$algorithm, see figure 25, where it is useful to remember that $k_0 = k_2 + k_3$, figure 22. From the building blocks of the section 6.3,

JHEP06(2016)101

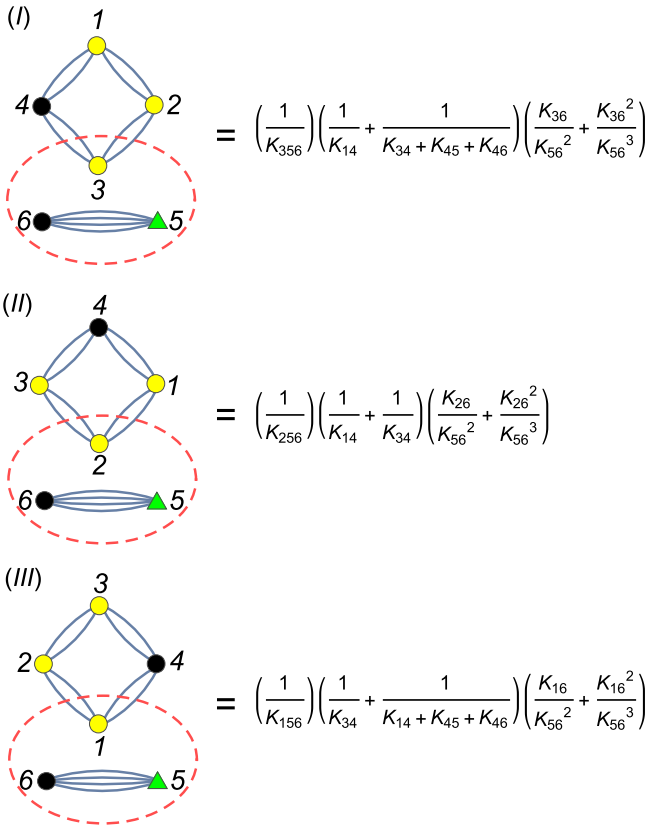

Figure 21. Results of the $(I), (II)$ and (III) configurations.

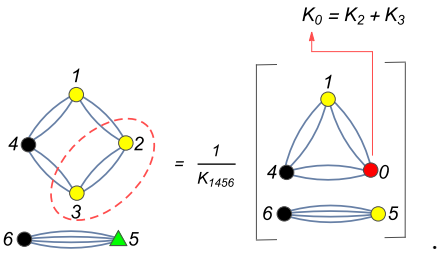

Figure 22. Computing the (a) configuration in figure 19.

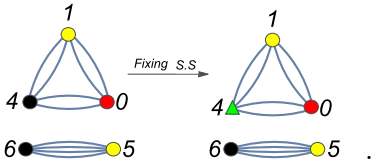

Figure 23. Gauging the Scale Symmetry (Iterative process).

JHEP06(2016)101

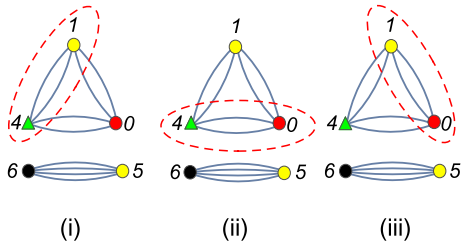

Figure 24. Allowable configurations 5-point graph (Iterative process).

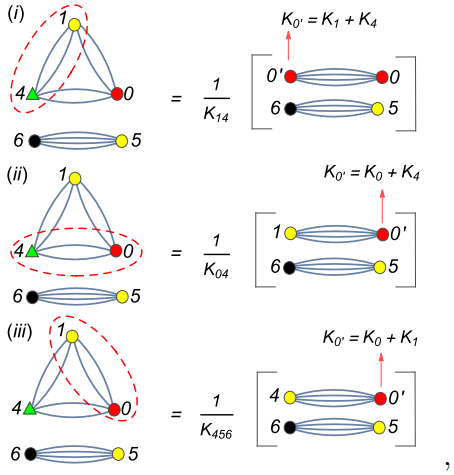

Figure 25. Allowable configurations five-point graph (Iterative process).

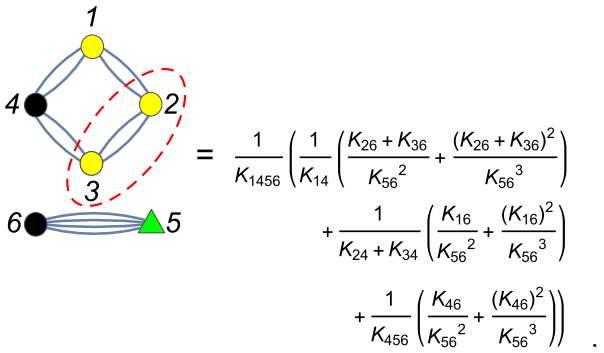

Figure 26. Result (a) configuration.

figure 10, we obtain the final answer for the (a) configuration in figure 19, see figure 26. Performing the same procedure for the (b) configuration one obtains the result given in figure 27.

Therefore, summing over all allowable configurations we obtain the total answer for the $\mathcal{I}_{(\mathcal{A})}$ graph, which is given by the non trivial expression

$$\begin{aligned}\mathcal{I}_{(\mathcal{A})} &= (I) + (II) + (III) + (\mathrm{a}) + (\mathrm{b}) \\ &= \frac{B[14:34+45+46]}{k_{356}}\frac{(k_{36})^2 B[56:36]}{(k_{56})^2} + \frac{B[14:34]}{k_{256}}\frac{(k_{26})^2 B[56:26]}{(k_{56})^2}\end{aligned}$$

JHEP06(2016)101

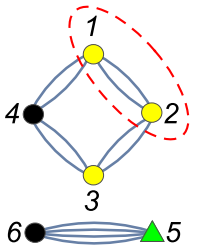

$$= \frac{1}{K_{3456}}\left(\frac{1}{K_{34}}\left(\frac{K_{36}+K_{46}}{K_{56}{}^2}+\frac{(K_{36}+K_{46})^2}{K_{56}{}^3}\right)+\frac{1}{K_{14}+K_{24}}\left(\frac{K_{36}}{K_{56}{}^2}+\frac{(K_{36})^2}{K_{56}{}^3}\right)+\frac{1}{K_{456}}\left(\frac{K_{46}}{K_{56}{}^2}+\frac{(K_{46})^2}{K_{56}{}^3}\right)\right).$$

Figure 27. Result (b) configuration.

$$\begin{aligned}
&+\frac{B[34:14+45+46]}{k_{156}}\,\frac{(k_{16})^2 B[56:16]}{(k_{56})^2} \\
&+\frac{1}{k_{1456}}\left[\frac{(k_{26}+k_{36})^2 B[56:26+36]}{k_{14}(k_{56})^2}+\frac{(k_{16})^2 B[56:16]}{(k_{24}+k_{34})(k_{56})^2}+\frac{(k_{46})^2 B[56:46]}{k_{456}(k_{56})^2}\right] \\
&+\frac{1}{k_{3456}}\left[\frac{(k_{36}+k_{46})^2 B[56:36+46]}{k_{34}(k_{56})^2}+\frac{(k_{36})^2 B[56:36]}{(k_{14}+k_{24})(k_{56})^2}+\frac{(k_{46})^2 B[56:46]}{k_{456}(k_{56})^2}\right],
\end{aligned} \tag{7.1}$$

where we have defined

$$B[A+B+\cdots I:C+B+\cdots J] := \frac{1}{k_A+k_B+\cdots k_I}+\frac{1}{k_C+k_D+\cdots k_J}, \tag{7.2}$$

and the labels A, B, C, D, I and J mean a index set, for example $k_A := k_{a_1\cdots a_m}$.

The (7.1) result was checked numerically.

7.1.2 $\mathcal{I}_{(\mathcal{B})}$-computation (general KLT and Λ algorithms)

In section 6.3 we have combined the general KLT algorithm [17] and the $\Lambda-$algorithm, respectively, in order to compute the (V) building block, however, in this section our idea is the opposite. First, we apply the $\Lambda-$algorithm as far as it is possible. From this method we will obtain subdiagrams with less vertices than the original one. Second, we perform the general KLT algorithm on these subdiagrams and finally we will be able to use the $\Lambda-$algorithm, again, to compute the diagrams into the vectors and matrix, such as it was done in section 6.3.1.

Let us remember that in the general KLT algorithm [17] one must find a base, left $(\mathcal{L})$ and right $(\mathcal{R})$, such that all graphs have a Hamiltonian decomposition, i.e. the integrands are product of two Parke-Taylor factors. One of its main drawback is to compute the inverse of the Gram matrix given by the product among the left and right base, $m^{\mathcal{L}|\mathcal{R}}$. For example, in six-point it is necessary to invert a 6×6 matrix.

However, since our idea is first to apply the $\Lambda-$algorithm then this drawback is softened.

Let us consider the $\mathcal{I}_{(\mathcal{B})}$ example in figure 16. In order to avoid singular allowable configurations we set the gauge fixing given in figure 28. There are only three non-zero allowable configurations, which are shown in figure 29. Since these three configurations are

JHEP06(2016)101

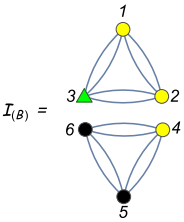

Figure 28. Gauge Fixing.

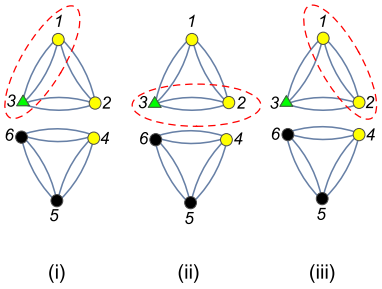

Figure 29. Non-zero configurations.

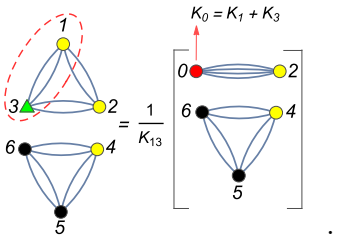

Figure 30. Computing the (i) configuration.

the same up to relabel the (1,2,3) vertices then it is enough just to compute one of them, for example we choose the first one, (i) configuration. Following the techniques presented in the section 7.1.1 one obtains the decomposition in figure 30. The 5 point graph on the right hand side can not be computed using the $\Lambda-$algorithm presented in section 6.2, therefore we use the general KLT-algorithm [17].

Following the same procedure used to compute the (V) building block in figure 8 (general KLT algorithm), we must break the 5 point graph (4-regular graph) into two 2-regular graphs (Left and Right) given in figure 31, where we have fixed the vertex number 5 using the scale symmetry. We choose the left and right base as[7] in figure 32, such that the diagrams in the $(L\mathcal{I}_{\mathcal{L}})$ and $(R\mathcal{I}_{\mathcal{R}})$ vectors have a Hamiltonian decomposition [58, 59]. Thus, we can write the 5-point diagram in figure 31 as the matrix product $(L\mathcal{I}_{\mathcal{L}})(m^{L|R})^{-1}(R\mathcal{I}_{\mathcal{R}})$, diagrammatically one can see it in figure 33. Using the $\Lambda-$algorithm we compute each diagram in figure 33, and the result is given in figure 34.

[7]Unlike of the general KLT algorithm presented in [17], we must keep the initial gauge fixing. This is important because the $\Lambda-$algorithm has generated a massive particle (red vertex).

JHEP06(2016)101

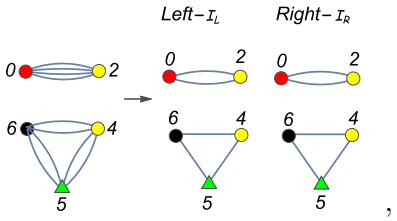

Figure 31. Splitting the 5 point 4-regular graph in two 2-regular graphs (Left and Right). The "5" vertex has been fixed by the scale symmetry.

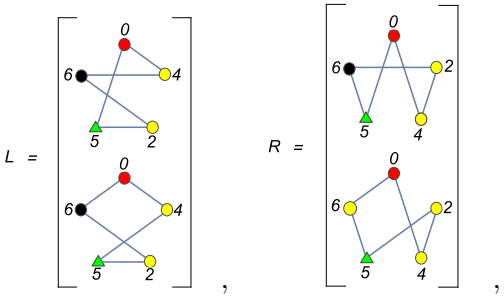

Figure 32. Left and Right base.

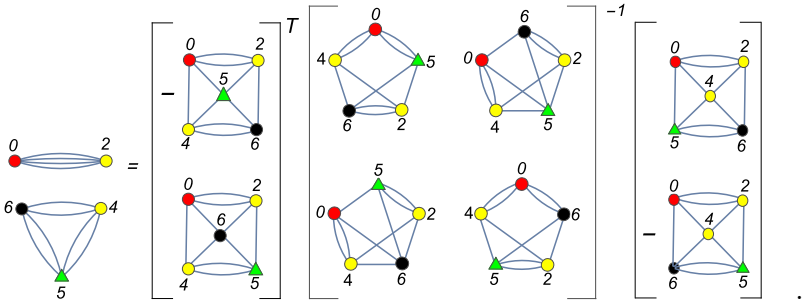

Figure 33. General KLT algorithm.

$$
\begin{pmatrix} 0 & 2 \\ 6 & 4 \\ & 5 \end{pmatrix} = \begin{pmatrix} \frac{-1}{K_{46}\,K_{456}} \\ \frac{1}{K_{45}\,(K_{46}+K_{56})} + \frac{1}{(K_{06}+K_{26})\,K_{456}} \end{pmatrix}^{T} \left[\begin{pmatrix} \frac{B[05:256]}{K_{26}} & \frac{1}{K_{25}\,(K_{26}+K_{56})} + \frac{1}{(K_{06}+K_{46})\,K_{256}} \\ \frac{1}{K_{26}\,K_{256}} & \frac{B[26+56:06]}{K_{25}} + \frac{1}{(K_{06}+K_{46})\,K_{256}} \end{pmatrix}^{T} \right]^{-1} \begin{pmatrix} \frac{1}{K_{456}\,K_{56}} \\ \frac{-1}{K_{456}\,K_{56}} \end{pmatrix}
$$

Figure 34. Result from the general KLT algorithm.

JHEP06(2016)101

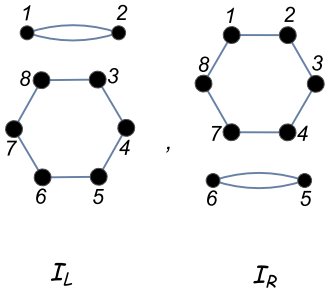

Figure 35. Left and Right base.

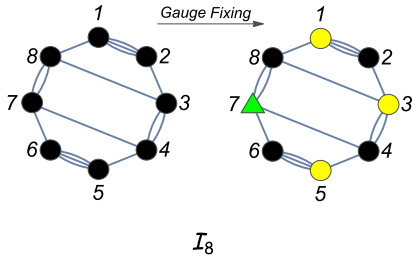

Figure 36. Gauge Fixing.

Relabeling the (1,2,3) indices one can write the final answer as

$$\mathcal{I}_{(\mathcal{B})} = \begin{pmatrix} \frac{-1}{k_{456}k_{46}} \\ \frac{1}{k_{456}(k_{16}+k_{26}+k_{36})} + \frac{1}{k_{45}(k_{46}+k_{56})} \end{pmatrix}^{\mathrm{T}} \tag{7.3}$$
$$\times \left[\frac{1}{k_{13}} \begin{pmatrix} \frac{B[15+35:256]}{k_{26}} & \frac{1}{k_{26}k_{256}} \\ \frac{1}{k_{25}(k_{26}+k_{56})} + \frac{1}{k_{256}(k_{16}+k_{36}+k_{46})} & \frac{1}{k_{256}(k_{16}+k_{36}+k_{46})} + \frac{B[16+36:26+56]}{k_{25}} \end{pmatrix}^{-1} \right.$$
$$+ \frac{1}{k_{23}} \begin{pmatrix} \frac{B[25+35:156]}{k_{16}} & \frac{1}{k_{16}k_{156}} \\ \frac{1}{k_{15}(k_{16}+k_{56})} + \frac{1}{k_{156}(k_{26}+k_{36}+k_{46})} & \frac{1}{k_{156}(k_{26}+k_{36}+k_{46})} + \frac{B[26+36:16+56]}{k_{15}} \end{pmatrix}^{-1}$$
$$\left. + \frac{1}{k_{12}} \begin{pmatrix} \frac{B[25+15:156]}{k_{36}} & \frac{1}{k_{36}k_{356}} \\ \frac{1}{k_{35}(k_{36}+k_{56})} + \frac{1}{k_{356}(k_{26}+k_{16}+k_{46})} & \frac{1}{k_{356}(k_{26}+k_{16}+k_{46})} + \frac{B[26+16:36+56]}{k_{35}} \end{pmatrix}^{-1} \right] \begin{pmatrix} \frac{1}{k_{456}k_{56}} \\ \frac{-1}{k_{456}k_{56}} \end{pmatrix},$$

which was checked numerically.

7.2 Eight-point

In this section we consider a non-trivial 8 point graph, which has the left and right decomposition as in figure 35. In addition to continue testing the power of the algorithm, this kind of graph was chosen in order to use the (V) building block (figure 8).

First we fix a gauge such that there is no a singular configuration, for example we choose the gauge fixing as in figure 36. Using this gauge we find three types of non-zero allowable configurations, see figure 37. Applying the $\Lambda-$algorithm one obtains that from the Type (I), $\{(a),(b)\}$, arises a 6-point subdiagrams with the graph given in figure 38, where we have fixed the "a"-puncture (by scale symmetry) in order to avoid singular

JHEP06(2016)101

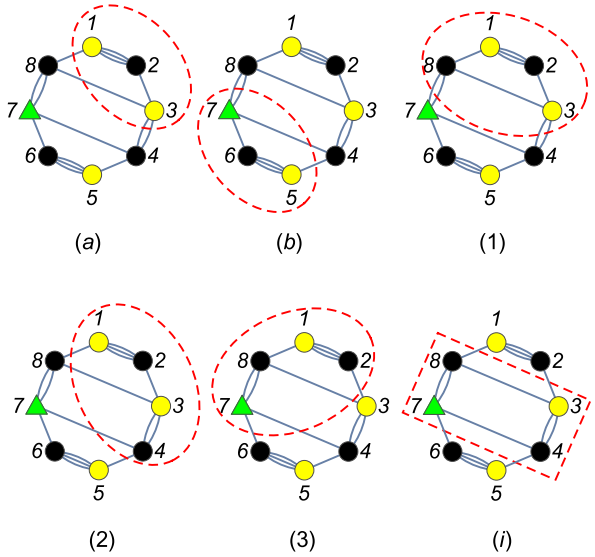

Figure 37. Non-zero allowable configurations. Type (I): (a) and (b) configurations. Type (II): (1), (2) and (3) configurations. Type(III): (i) configuration.

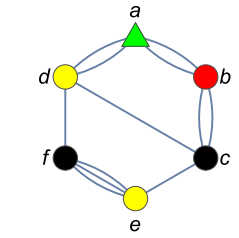

Figure 38. Six point graph from the Type (I) configuration.

configurations. This graph is very similar to one given in figure 17 and its computation is totally analog. Using the $\Lambda-$algorithm the result for this graph is the function

$$\begin{aligned} F_{ab}(k_a,k_b,k_c,k_d,k_e,k_f) = &-\left(\frac{k_{df}B[ef:df]}{k_{ab}(k_{ac}+k_{bc})k_{ef}}+\frac{(k_{af}+k_{bf}+k_{df})B[ef:af+bf+df]}{k_{ab}k_{cef}k_{ef}}\right)\\ &-\left(\frac{(k_{af}+k_{df})B[ef:af+df]}{k_{ad}k_{bc}k_{ef}}+\frac{(k_{af}+k_{bf}+k_{df})B[ef:af+bf+df]}{k_{ad}k_{cef}k_{ef}}\right)\\ &-\frac{k_{df}B[bc:cd+ce+cf]B[ef:df]}{k_{abc}kef}\,. \end{aligned} \tag{7.4}$$

Therefore, the (a) and (b) configurations can be written as

$$\text{(a)} = -\frac{k_{23}B[12:23]}{k_{123}k_{12}}F_{ab}(k_8,k_1+k_2+k_3,k_4,k_7,k_5,k_6), \tag{7.5}$$

$$\text{(b)} = -\frac{k_{57}B[56:57]}{k_{567}k_{56}}F_{ab}(k_4,k_5+k_6+k_7,k_8,k_3,k_1,k_2). \tag{7.6}$$

From the type (II) configurations, $\{(1),(2),(3)\}$, one obtains the following 5-point sub-diagrams in figure 39 after applying the $\Lambda-$algorithm. The first one, $F^5_{13}(k_a,k_b,k_c,k_d,k_e)$,

JHEP06(2016)101

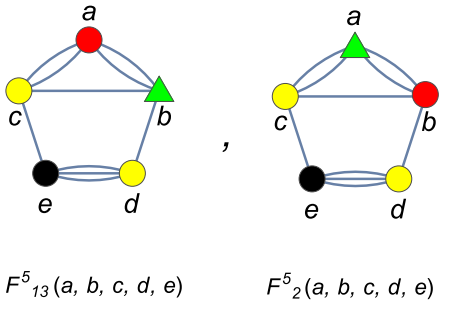

Figure 39. Five point graphs from the Type(II) configurations.

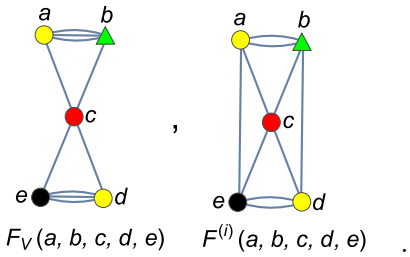

Figure 40. Five point graphs from Type(III) configuration.

is a subdiagram obtained from the (1) and (3) configurations and the second one, $F_2^5(k_a, k_b, k_c, k_d, k_e)$, is obtained from the (2) configuration. These two subdiagrams are very similar to one obtained in figure 23 and their computations are very simple using the $\Lambda-$algorithm. The results for these two graphs are

$$F_{13}^5(k_a, k_b, k_c, k_d, k_e) = -\frac{k_{ce}B[de:ce]}{k_{ab}k_{de}} - \frac{(k_{ae}+k_{ce})B[de:ae+ce]}{k_{bde}k_{de}}, \tag{7.7}$$

$$F_2^5(k_a, k_b, k_c, k_d, k_e) = -\frac{k_{ce}B[de:ce]}{k_{ab}k_{de}} - \frac{(k_{ae}+k_{ce})B[de:ae+ce]}{k_{ac}k_{de}}. \tag{7.8}$$

Note that the two answers are totally different, this is because $k_{ac} \neq k_{bde}$ since there is a massive particle. We can now write the results for the Type (II) configurations, $\{(1),(2),(3)\}$, as

$$(1) = \frac{F_{13}^5(k_4+k_5+k_6+k_7, k_8, k_3, k_1, k_2)F_{13}^5(k_1+k_2+k_3+k_8, k_4, k_7, k_5, k_6)}{k_{4567}}, \tag{7.9}$$

$$(2) = \frac{F_2^5(k_4, k_5+k_6+k_7+k_8, k_3, k_1, k_2)F_2^5(k_8, k_1+k_2+k_3+k_4, k_7, k_5, k_6)}{k_{5678}}, \tag{7.10}$$

$$(3) = \frac{F_{13}^5(k_7, k_8, k_3+k_4+k_5+k_6, k_1, k_2)F_{13}^5(k_3, k_4, k_1+k_2+k_7+k_8, k_5, k_6)}{k_{4567}}. \tag{7.11}$$

Finally, from the Type (III) configuration, $\{(i)\}$, one obtains the subdiagrams in figure 40. The first one, $F_V(k_a, k_b, k_c, k_d, k_e)$, is the (V) building block computed in section 6.3.1 and it is given by

$$F_V(k_a, k_b, k_c, k_d, k_e) = \left(\frac{1}{k_{ab}k_{de}}\right)^2 (k_{ae}k_{bd} - k_{bce}k_{be}). \tag{7.12}$$

JHEP06(2016)101

The second one was also computed in section 6.3.1 using the Λ−algorithm and its result is very simple

$$F^{(i)}(k_a,k_b,k_c,k_d,k_e)=\frac{1}{k_{ab}k_{de}}. \tag{7.13}$$

Thus, the (i) configuration can be read as

$$(i)=\frac{F_V(k_1,k_2,k_3+k_4+k_7+k_8,k_5,k_6)\;F^{(i)}(k_7,k_8,k_1+k_2+k_5+k_6,k_3,k_4)}{k_{3478}} \tag{7.14}$$

The full answer is the sum over all configurations given in figure 37, i.e.

$$\begin{aligned}\mathcal{I}_8&=(\mathrm{a})+(\mathrm{b})+(1)+(2)+(3)+(i) \qquad (7.15)\\ &=-\frac{k_{23}B[12:23]}{k_{123}k_{12}}F_{ab}(k_8,k_1+k_2+k_3,k_4,k_7,k_5,k_6)\\ &\quad-\frac{k_{57}B[56:57]}{k_{567}k_{56}}F_{ab}(k_4,k_5+k_6+k_7,k_8,k_3,k_1,k_2)\\ &\quad+\frac{F^5_{13}(k_4+k_5+k_6+k_7,k_8,k_3,k_1,k_2)F^5_{13}(k_1+k_2+k_3+k_8,k_4,k_7,k_5,k_6)}{k_{4567}}\\ &\quad+\frac{F^5_{2}(k_4,k_5+k_6+k_7+k_8,k_3,k_1,k_2)F^5_{2}(k_8,k_1+k_2+k_3+k_4,k_7,k_5,k_6)}{k_{5678}}\\ &\quad+\frac{F^5_{13}(k_7,k_8,k_3+k_4+k_5+k_6,k_1,k_2)F^5_{13}(k_3,k_4,k_1+k_2+k_7+k_8,k_5,k_6)}{k_{4567}}\\ &\quad+\frac{F_V(k_1,k_2,k_3+k_4+k_7+k_8,k_5,k_6)\;F^{(i)}(k_7,k_8,k_1+k_2+k_5+k_6,k_3,k_4)}{k_{3478}}.\end{aligned}$$

This result was checked numerically.

8 The Baadsgaard, Bohr, Bourjaily and Damgaard Rules (BBBD) vs the Λ-algorithm

In [18], Baadsgaard et al., formulated some rules in order to compute the same kind of integrals or diagrams that we have studied so far. Nevertheless, although their rules are a certain sum over all possible factorization limits, similar to the Λ-algorithm, these two algorithms present important differences. For example, the Λ-algorithm depends of the gauge fixing, such as it has been explained and shown in section 6. This particular characteristic is in fact a powerful tool, for instance, using the BBBD rules, which are independent of the choice of gauge, it is not possible to compute directly integrands such as ones given by the diagrams in figures 17, 23, 36, 38 or 39. The reason is because there are four or three edges connecting two vertices. Nevertheless, as it has already been shown, these kind of diagrams can be easily computed using the Λ-algorithm.

At the same way as in [18], the Λ-algorithm can also be directly used to integrands with non trivial numerator. For example, let us consider the same diagram as in [18], see figure 41, where the black dotted line counts as negative solid line (antiline), i.e. it carries negative weight. Clearly this diagram corresponds to the integrand

$$H^{\mathcal{N}_6}=\frac{(\tau_{1:2}\tau_{2:3}\tau_{3:4}\tau_{4:5}\tau_{5:6}\tau_{6:1})(\tau_{1:2}\tau_{2:3}\tau_{3:5}\tau_{5:6}\tau_{6:1})(\tau_{2:4}\tau_{4:6}\tau_{6:2})}{(\tau_{2:6}\tau_{6:2})}, \tag{8.1}$$

JHEP06(2016)101

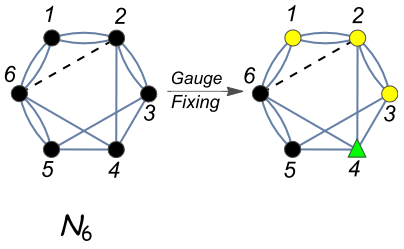

Figure 41. Gauge fixing for the $\mathcal{N}_6$ numerator diagram.

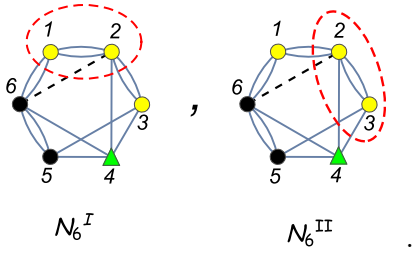

Figure 42. Non zero configurations for the $\mathcal{N}_6$ diagram.

or using the CHY variables one can write it as

$$H_{\rm CHY}^{\mathcal{N}_6} = \frac{(z_2 - z_6)}{(z_1-z_2)^2(z_1-z_6)^2(z_2-z_3)^2(z_5-z_6)^2(z_2-z_4)(z_3-z_4)(z_3-z_5)(z_4-z_5)(z_4-z_6)}.$$

Note that the lines and the antilines connecting the same two vertices cancel each other.[8] Moreover, due to the presence of a non trivial numerator, the denominator has more factors than otherwise, this is so as to retain the $\mathrm{SL}(2,\mathbb{C})$ invariance.

Obviously, the $\mathcal{N}_6$ diagram in figure 41 is not a 4-regular graph, but the subtraction between the number of lines and antilines must always be four (on each vertex) in order to keep the $\mathrm{SL}(2,\mathbb{C})$ symmetry.

To compute the $\mathcal{N}_6$ diagram we are obliged to extend the Λ-Theorem

- **Λ-theorem (extension).**
  Let C be an allowable configuration, then the integrand $\mathcal{I} = |ijk|\Delta_{FP}(ijk,d)\,H(\sigma)$ on the C configuration has the $\Lambda-$behavior

$$\mathcal{I}\Big|^{C}_{\Lambda\to 0} \sim \Lambda^{(L-A)-4} + \mathcal{O}(\Lambda^{(L-A)-3}), \tag{8.2}$$

  around $\Lambda = 0$, where L is the number of lines and A is the number of antilines which are intersected by the red line.

Using the **Λ-theorem (extension).** it is simple to see there are only two non zero allowable configurations given in figure 42. These two configurations are easily calculated from the rules in section 6.2, so the first one configuration reads

$$\mathcal{N}_6^I = \frac{1}{k_{3456}\,k_{456}\,k_{56}}\ , \tag{8.3}$$

[8] This fact means that a numerator cancels with one denominator.

JHEP06(2016)101

and the second one as

$$\mathcal{N}_6^{II} = \frac{1}{k_{1456}}\left[\frac{1}{k_{456}\,k_{56}} + \frac{1}{k_{156}}\left(\frac{1}{k_{56}} + \frac{1}{k_{16}}\right)\right]. \tag{8.4}$$

Therefore, the final result can be written

$$\mathcal{N}_6 = \mathcal{N}_6^{I} + \mathcal{N}_6^{II} \tag{8.5}$$

$$= \frac{1}{k_{3456}\,k_{456}\,k_{56}} + \frac{1}{k_{1456}}\left[\frac{1}{k_{456}\,k_{56}} + \frac{1}{k_{156}}\left(\frac{1}{k_{56}} + \frac{1}{k_{16}}\right)\right], \tag{8.6}$$

which is the same answer found in [18].

This show how powerful is the $\Lambda-$algorithm, which can be applied to solve highly non trivial integrands.

9 Discussions

In this paper we gave a new representation for the CHY integrals. We call this new representation as the $\Lambda-$prescription. The $\Lambda-$prescription is supported on an algebraic curve of degree two, which is embedded in $\mathbb{C}P^2$, i.e. this is a sphere. This curve can be thought as a Riemann surface with two sheets connected by a branch cut.

The new scattering equations (*the* Λ*-scattering equations*) must contain information about the branch where the particles (punctures) are localized. For example, the Λ scattering equations are given by the expression

$$E_a := \sum_{b\neq a}^{n} k_a \cdot k_b\, \tau_{a:b}, \quad \text{where } \tau_{a:b} := \frac{1}{2\,y_a}\left(\frac{y_a + y_b + \sigma_{ab}}{\sigma_{ab}}\right), \quad \text{and } y_a^2 = \sigma_a^2 - \Lambda^2,$$

with $a = 1, \ldots n$. When $y_a = \sqrt{\sigma_a^2 - \Lambda^2}$ one says that the particle (puncture) is on the upper sheet and when $y_a = -\sqrt{\sigma_a^2 - \Lambda^2}$ then one says that the particle is on the lower sheet. Note that the quadratic curves, y_a, have an additional parameter, Λ, which controls the opening of the branch cut. When this parameter is promoted as a variable then a new symmetry arise (scale symmetry), which can be used to fix one more particle (puncture).

In section 5 we performed the global residue theorem over this new variable, Λ. After integrating Λ one obtains that the Λ prescription must be evaluated at the point $\Lambda = 0$ ($\Lambda = \infty$), i.e. at the limit when the branch cut collapses in a line. So, the initial integral is broken into two new smaller integrals, which are now written as in the original CHY approach. In addition, these two new integrals are multiplied by a propagator, which is associated to the collapsed branch cut, it is kind a factorization limit. This is an iterative process, i.e. it can be applied over each one of these two new integrals. All this procedure is encoded into what we call the Λ*-algorithm.*

The $\Lambda-$algorithm allow us to expand a given integral in terms of fundamental building blocks, given in figure 8.

Unlike to the other algorithms, the $\Lambda-$algorithm depends totally of the gauge fixing. Although this does not look like to be a good thing, in fact it is. For example, diagrams

JHEP06(2016)101

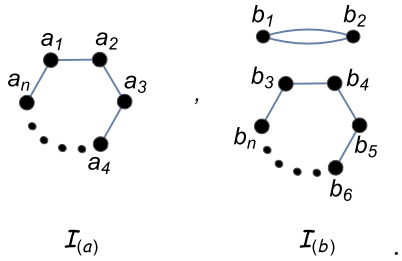

Figure 43. Two 2-regular graphs. $\mathcal{I}_a$ is a Parker-Taylor graph. $\mathcal{I}_b$ is a bubble with a regular polygon graph.

such as ones given in figure 16, which are very complicated using other type of algorithms, they are easily computed from the Λ algorithm, obviously, after choosing a good gauge.

The Λ algorithm is a powerful, simple and beautiful tool because it is a pictorial algorithm. Nevertheless, this mechanism has some limitations, i.e. there are some CHY integrals which can not be performed just using this algorithm. This is due we do not know the behavior of the *singular allowable configurations*, which is the reason why one must choose a good gauge. It will be very interesting to know how to extend the Λ algorithm to singular allowable configurations.

We know that the Λ algorithm can be used on a big spectrum of CHY integrals, the main idea is to choose a gauge such that the all allowable configurations will not be singular. In particular, we know diagrams on which this fact always happens. These diagrams are given by all possible combinations of the two 2-regular graphs in figure 43. The $\mathcal{I}_a$ graph is clearly a Parker-Taylor factor, therefore, the diagram given by the integrand $H(\sigma) = \mathcal{I}_a\, \mathcal{I}_a$ is just the $m(\alpha|\beta)$ kernel, which is very simple to compute. The other two options given by the integrands $H(\sigma) = \mathcal{I}_a\, \mathcal{I}_b$ and $H(\sigma) = \mathcal{I}_b\, \mathcal{I}_b$, which are non trivial diagrams, they can be easily computed using the Λ algorithm.

The Λ algorithm has two more advantages. As we saw, some massive particles arise in the process, so this algorithm supports off shell particles. The other one is that this algorithm could be used on integrands with non trivial numerators, such as one given in figure 41. These two characteristics are very important in order to compute diagrams at loop level, for example, the diagram given by figure 44, which appears at 1-loop computation of the 5-gon, it can easily be computed using the $\Lambda-$algorithm [60].

Finally, note that the integrand in the Λ prescription is basically obtained from the original CHY approach just changing the $\frac{1}{z_{ab}}$ form by the $\tau_{a:b}$ form. However, although $\frac{1}{z_{ab}}$ is an antisymmetric form, i.e $\frac{1}{z_{ab}} = -\frac{1}{z_{ba}}$, the $\tau_{a:b}$ form is not, $\tau_{a:b} \neq -\tau_{a:b}$. So, the antisymmetric matrix, $\Psi_{\alpha\beta}$, which was defined in [1], it is not any more antisymmetric when $(z_{ab})^{-1}$ is replaced by τ_{ab}. Therefore, the Pfaffian of $\Psi_{\alpha\beta}(\tau_{a:b})$ is not well defined. Naively, in order to give an interpretation for the Yang-Mills theory from the Λ prescription one can replace the Pfaffian of $\Psi_{\alpha\beta}(z_{a:b})$ by $\sqrt{\det\left(\Psi_{\alpha\beta}(\tau_{a:b})\right)}$, but we leave this for future research.

JHEP06(2016)101

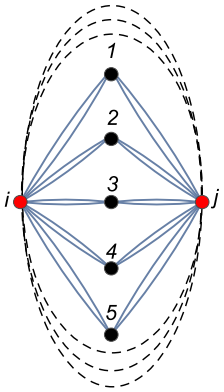

Figure 44. 5-gon CHY diagram representation.

Acknowledgments

The author would like to thank F. Cachazo for his initial collaboration in this paper. The author thanks to F. Cachazo, C. Cardona and C. Kalousios for carefully reading the draft, for comment and useful discussion. The author would like to thank the hospitality of Perimeter Institute, Universidade de São Paulo (USP) and Universidad Santigo de Cali, where this work was developed. The author thanks to the string theory group of the USP, where this work was presented. HG is supported by CNPq grant 403178/2014-2 and USC grant DGI-COCEIN-No 935-621115-N22.

A Λ-theorem

In this appendix we prove the Λ-theorem, which was given in section 6.1.1.

Λ-theorem. Let C be an allowable configuration, then the integrand $\mathcal{I} = |ijk|\Delta_{FP}(ijk,d)H^D(\sigma)$ on the C configuration has the $\Lambda-$behavior

$$\mathcal{I}\Big|^{C}_{\Lambda\to 0} \sim \Lambda^{L-4} + \mathcal{O}(\Lambda^{L-3})$$

around $\Lambda = 0$, where L is the number of edges which are intersected by the red line.

Proof. Let us consider an allowable configuration, i.e. two fixed punctures on the upper branch and the others two fixed punctures on the lower branch. Without loss of generality, one can consider the 1 and 2 puntures fixed on the upper branch and the 3 and 4 puntures fixed on the lower branch. Under this consideration it is straightforward to check that the Faddeev-Popov determinant has a behavior

$$|1,2,3|\Delta_{FP}(1,2,3|4) = \frac{2^5\,\sigma_1^2\,\sigma_2^2\,\sigma_3^3\,\sigma_4\,(\sigma_1-\sigma_2)^2(\sigma_3-\sigma_4)}{\Lambda^4} - \frac{1}{\sigma_4\,\Lambda^2} + \mathcal{O}(\Lambda^0). \tag{A.1}$$

Before showing that $H^D(\sigma) \sim \Lambda^L$, we analyse the $\tau_{a:b}$ form. When the σ_a and σ_b punctures are on upper sheet, i.e. $y_a = \sqrt{\sigma_a^2-\Lambda^2}$ and $y_b = \sqrt{\sigma_b^2-\Lambda^2}$, the $\tau_{a:b}$ form has the behavior

$$\tau_{a:b}\Big|^{a,b} = \frac{1}{\sigma_{ab}} - \frac{\Lambda^2}{4\,\sigma_a^2\,\sigma_b} - \frac{(\sigma_a^2+\sigma_a\,\sigma_b+3\,\sigma_b^2)\Lambda^4}{2^4\,\sigma_a^4\,\sigma_b^3} + \mathcal{O}(\Lambda^6), \tag{A.2}$$

JHEP06(2016)101

where $\tau_{a:b}\Big|^{a,b}$ means that σ_a and σ_b are on the upper branch cut. For the others three more configurations, $(a \to \text{upper}, b \to \text{lower})$, $(a \to \text{lower}, b \to \text{upper})$ and $(a \to \text{lower}, b \to \text{lower})$, the Λ expansion is read as

$$\begin{aligned}
\tau_{a:b}\Big|^{a}_{\ b} &= \frac{1}{\sigma_a} + \frac{(\sigma_a + 2\sigma_b)\Lambda^2}{2^2\,\sigma_a^3\sigma_b} + \frac{(\sigma_a^3 + \sigma_a^2\sigma_b + 3\sigma_a\sigma_b^2 + 6\sigma_b^3)\Lambda^4}{2^4\,\sigma_a^5\sigma_b^3} + \mathcal{O}(\Lambda^6), \\
\tau_{a:b}\Big|^{\ b}_{a} &= \frac{\Lambda^2}{2^2\,\sigma_a^2\sigma_b} + \frac{(\sigma_a^2 + \sigma_a\sigma_b + 3\sigma_b^2)\Lambda^4}{2^4\,\sigma_a^4\sigma_b^3} + \mathcal{O}(\Lambda^6), \\
\tau_{a:b}\Big|_{a,b} &= \frac{\sigma_b}{\sigma_a^2 - \sigma_a\sigma_b} - \frac{(\sigma_a + 2\sigma_b)\Lambda^2}{2^2\,\sigma_a^3\sigma_b} - \frac{(\sigma_a^3 + \sigma_a^2\sigma_b + 3\sigma_a]\sigma_b^2 + 6\sigma_b^3)\Lambda^4}{2^4\,\sigma_a^5\sigma_b^3} + \mathcal{O}(\Lambda^6).
\end{aligned} \tag{A.3}$$

Now, let us remember that the $H^D(\sigma)$ integrand is given by the products of chains, i.e. the products of factors such as

$$[a_1, \ldots a_k] = (\tau_{a_1:a_2}\,\tau_{a_2:a_3}\,\cdots\,\tau_{a_{k-1}:a_k}\,\tau_{a_k:a_1}). \tag{A.4}$$

This implies the number of edges which are intersected by the red line is a even number, it is because for each $\tau_{a_i:a_j}\Big|^{a_i}_{a_j}$ term into the chain, it must also have a term such as $\tau_{a_m:a_n}\Big|^{a_n}_{a_m}$, in order to close it. So, from this fact and using the Λ expansion given in (A.2) and (A.3), it is straightforward to conclude that

$$H^D(\sigma) \sim \Lambda^L, \tag{A.5}$$

where L is the number of edges which are intersected by the red line. Thus the $\Lambda-$theorem has been proved ■

The proof for the $\Lambda-$theorem (Extension), given in section 8, is completely analogous.

Open Access. This article is distributed under the terms of the Creative Commons Attribution License (CC-BY 4.0), which permits any use, distribution and reproduction in any medium, provided the original author(s) and source are credited.

References

[1] F. Cachazo, S. He and E.Y. Yuan, *Scattering of massless particles in arbitrary dimensions*, *Phys. Rev. Lett.* **113** (2014) 171601 [arXiv:1307.2199] [INSPIRE].

[2] F. Cachazo, S. He and E.Y. Yuan, *Scattering of massless particles: scalars, gluons and gravitons*, *JHEP* **07** (2014) 033 [arXiv:1309.0885] [INSPIRE].

[3] F. Cachazo, S. He and E.Y. Yuan, *Scattering equations and matrices: from Einstein to Yang-Mills, DBI and NLSM*, *JHEP* **07** (2015) 149 [arXiv:1412.3479] [INSPIRE].

[4] L. Mason and D. Skinner, *Ambitwistor strings and the scattering equations*, *JHEP* **07** (2014) 048 [arXiv:1311.2564] [INSPIRE].

[5] L. Dolan and P. Goddard, *Proof of the formula of Cachazo, He and Yuan for Yang-Mills tree amplitudes in arbitrary dimension*, *JHEP* **05** (2014) 010 [arXiv:1311.5200] [INSPIRE].

JHEP06(2016)101

[6] N. Berkovits, *Infinite tension limit of the pure spinor superstring*, *JHEP* **03** (2014) 017 [arXiv:1311.4156] [INSPIRE].

[7] T. Adamo, E. Casali and D. Skinner, *Ambitwistor strings and the scattering equations at one loop*, *JHEP* **04** (2014) 104 [arXiv:1312.3828] [INSPIRE].

[8] H. Gomez and E.Y. Yuan, *N-point tree-level scattering amplitude in the new Berkovits' string*, *JHEP* **04** (2014) 046 [arXiv:1312.5485] [INSPIRE].

[9] L. Dolan and P. Goddard, *The polynomial form of the scattering equations*, *JHEP* **07** (2014) 029 [arXiv:1402.7374] [INSPIRE].

[10] Y. Geyer, A.E. Lipstein and L.J. Mason, *Ambitwistor strings in four dimensions*, *Phys. Rev. Lett.* **113** (2014) 081602 [arXiv:1404.6219] [INSPIRE].

[11] F. Cachazo, S. He and E.Y. Yuan, *Einstein-Yang-Mills scattering amplitudes from scattering equations*, *JHEP* **01** (2015) 121 [arXiv:1409.8256] [INSPIRE].

[12] K. Ohmori, *Worldsheet geometries of ambitwistor string*, *JHEP* **06** (2015) 075 [arXiv:1504.02675] [INSPIRE].

[13] E. Casali, Y. Geyer, L. Mason, R. Monteiro and K.A. Roehrig, *New ambitwistor string theories*, *JHEP* **11** (2015) 038 [arXiv:1506.08771] [INSPIRE].

[14] P. Griffiths and J. Harris, *Principles of algebrais geometry*, Wiley, U.S.A. (1994).

[15] C. Kalousios, *Massless scattering at special kinematics as Jacobi polynomials*, *J. Phys.* **A 47** (2014) 215402 [arXiv:1312.7743] [INSPIRE].

[16] C. Kalousios, *Scattering equations, generating functions and all massless five point tree amplitudes*, *JHEP* **05** (2015) 054 [arXiv:1502.07711] [INSPIRE].

[17] F. Cachazo and H. Gomez, *Computation of contour integrals on* $\mathcal{M}_{0,n}$, *JHEP* **04** (2016) 108 [arXiv:1505.03571] [INSPIRE].

[18] C. Baadsgaard, N.E.J. Bjerrum-Bohr, J.L. Bourjaily, P.H. Damgaard and B. Feng, *Integration rules for loop scattering equations*, *JHEP* **11** (2015) 080 [arXiv:1508.03627] [INSPIRE].

[19] C. Baadsgaard, N.E.J. Bjerrum-Bohr, J.L. Bourjaily and P.H. Damgaard, *Scattering equations and Feynman diagrams*, *JHEP* **09** (2015) 136 [arXiv:1507.00997] [INSPIRE].

[20] C. Cardona and C. Kalousios, *Comments on the evaluation of massless scattering*, *JHEP* **01** (2016) 178 [arXiv:1509.08908] [INSPIRE].

[21] C. Cardona and C. Kalousios, *Elimination and recursions in the scattering equations*, *Phys. Lett.* **B 756** (2016) 180 [arXiv:1511.05915] [INSPIRE].

[22] R. Huang, J. Rao, B. Feng and Y.-H. He, *An algebraic approach to the scattering equations*, *JHEP* **12** (2015) 056 [arXiv:1509.04483] [INSPIRE].

[23] C.S. Lam and Y.-P. Yao, *Evaluation of the Cachazo-He-Yuan gauge amplitude*, *Phys. Rev.* **D 93** (2016) 105008 [arXiv:1602.06419] [INSPIRE].

[24] S. Weinzierl, *On the solutions of the scattering equations*, *JHEP* **04** (2014) 092 [arXiv:1402.2516] [INSPIRE].

[25] C.R. Mafra, *Berends-Giele recursion for double-color-ordered amplitudes*, arXiv:1603.09731 [INSPIRE].

JHEP06(2016)101

[26] T. Adamo and E. Casali, *Scattering equations, supergravity integrands and pure spinors*, *JHEP* **05** (2015) 120 [arXiv:1502.06826] [INSPIRE].

[27] E. Casali and P. Tourkine, *Infrared behaviour of the one-loop scattering equations and supergravity integrands*, *JHEP* **04** (2015) 013 [arXiv:1412.3787] [INSPIRE].

[28] Y. Geyer, L. Mason, R. Monteiro and P. Tourkine, *Loop integrands for scattering amplitudes from the Riemann sphere*, *Phys. Rev. Lett.* **115** (2015) 121603 [arXiv:1507.00321] [INSPIRE].

[29] C. Baadsgaard, N.E.J. Bjerrum-Bohr, J.L. Bourjaily, P.H. Damgaard and B. Feng, *Integration rules for loop scattering equations*, *JHEP* **11** (2015) 080 [arXiv:1508.03627] [INSPIRE].

[30] C. Baadsgaard, N.E.J. Bjerrum-Bohr, J.L. Bourjaily, S. Caron-Huot, P.H. Damgaard and B. Feng, *New representations of the perturbative S-matrix*, *Phys. Rev. Lett.* **116** (2016) 061601 [arXiv:1509.02169] [INSPIRE].

[31] R. Huang, Q. Jin, J. Rao, K. Zhou and B. Feng, *The Q-cut representation of one-loop integrands and unitarity cut method*, *JHEP* **03** (2016) 057 [arXiv:1512.02860] [INSPIRE].

[32] B. Feng, *CHY-construction of planar loop integrands of cubic scalar theory*, *JHEP* **05** (2016) 061 [arXiv:1601.05864] [INSPIRE].

[33] Y. Geyer, L. Mason, R. Monteiro and P. Tourkine, *One-loop amplitudes on the Riemann sphere*, *JHEP* **03** (2016) 114 [arXiv:1511.06315] [INSPIRE].

[34] S. He and E.Y. Yuan, *One-loop scattering equations and amplitudes from forward limit*, *Phys. Rev.* **D 92** (2015) 105004 [arXiv:1508.06027] [INSPIRE].

[35] F. Cachazo, S. He and E.Y. Yuan, *One-loop corrections from higher dimensional tree amplitudes*, arXiv:1512.05001 [INSPIRE].

[36] D. Fairlie and D. Roberts, *Dual models without tachyons — a new approach*, unpublished, Durham preprint, (1972) [INSPIRE].

[37] D. Roberts, *Mathematical structure of dual amplitudes*, Ph.D. thesis, Durham University, Durham U.K. (1972), pg. 73.

[38] D.B. Fairlie, *A coding of real null four-momenta into world-sheet co-ordinates*, *Adv. Math. Phys.* **2009** (2009) 284689 [arXiv:0805.2263] [INSPIRE].

[39] D.J. Gross and P.F. Mende, *String theory beyond the Planck scale*, *Nucl. Phys.* **B 303** (1988) 407 [INSPIRE].

[40] E. Witten, *Parity invariance for strings in twistor space*, *Adv. Theor. Math. Phys.* **8** (2004) 779 [hep-th/0403199] [INSPIRE].

[41] P. Caputa and S. Hirano, *Observations on open and closed string scattering amplitudes at high energies*, *JHEP* **02** (2012) 111 [arXiv:1108.2381] [INSPIRE].

[42] P. Caputa, *Lightlike contours with fermions*, *Phys. Lett.* **B 716** (2012) 475 [arXiv:1205.6369] [INSPIRE].

[43] Y. Makeenko and P. Olesen, *The QCD scattering amplitude from area behaved Wilson loops*, *Phys. Lett.* **B 709** (2012) 285 [arXiv:1111.5606] [INSPIRE].

[44] F. Cachazo and Y. Geyer, *A 'twistor string' inspired formula for tree-level scattering amplitudes in $N = 8$ SUGRA*, arXiv:1206.6511 [INSPIRE].

JHEP06(2016)101

[45] S. Weinberg, *Infrared photons and gravitons*, *Phys. Rev.* **140** (1965) B516 [INSPIRE].

[46] F. Cachazo and A. Strominger, *Evidence for a new soft graviton theorem*, arXiv:1404.4091 [INSPIRE].

[47] C. Kalousios and F. Rojas, *Next to subleading soft-graviton theorem in arbitrary dimensions*, *JHEP* **01** (2015) 107 [arXiv:1407.5982] [INSPIRE].

[48] M. Zlotnikov, *Sub-sub-leading soft-graviton theorem in arbitrary dimension*, *JHEP* **10** (2014) 148 [arXiv:1407.5936] [INSPIRE].

[49] B.U.W. Schwab and A. Volovich, *Subleading soft theorem in arbitrary dimensions from scattering equations*, *Phys. Rev. Lett.* **113** (2014) 101601 [arXiv:1404.7749] [INSPIRE].

[50] N. Afkhami-Jeddi, *Soft graviton theorem in arbitrary dimensions*, arXiv:1405.3533 [INSPIRE].

[51] H. Kawai, D.C. Lewellen and S.-H. Henry Tye, *A relation between tree amplitudes of closed and open strings*, *Nucl. Phys.* **B 269** (1986) 1 [INSPIRE].

[52] Z. Bern, J.J.M. Carrasco and H. Johansson, *New relations for gauge-theory amplitudes*, *Phys. Rev.* **D 78** (2008) 085011 [arXiv:0805.3993] [INSPIRE].

[53] Z. Bern, L.J. Dixon, M. Perelstein and J.S. Rozowsky, *Multileg one loop gravity amplitudes from gauge theory*, *Nucl. Phys.* **B 546** (1999) 423 [hep-th/9811140] [INSPIRE].

[54] F. Cachazo, S. He and E.Y. Yuan, *Scattering equations and Kawai-Lewellen-Tye orthogonality*, *Phys. Rev.* **D 90** (2014) 065001 [arXiv:1306.6575] [INSPIRE].

[55] F. Cachazo and G. Zhang, *Minimal basis in four dimensions and scalar blocks*, arXiv:1601.06305 [INSPIRE].

[56] H. Ruegg and M. Ruiz-Altaba, *The Stueckelberg field*, *Int. J. Mod. Phys.* **A 19** (2004) 3265 [hep-th/0304245] [INSPIRE].

[57] S.J. Parke and T.R. Taylor, *An amplitude for n gluon scattering*, *Phys. Rev. Lett.* **56** (1986) 2459 [INSPIRE].

[58] J.L. Gross and J. Yellen, *Graph theory and its applications*, Chapman and Hall, London U.K. (2006).

[59] R. Diestel, *Graph theory*, third edition, Springer, Germany (2000).

[60] C. Cardona and H. Gomez, *Elliptic scattering equations*, arXiv:1605.01446 [INSPIRE].

JHEP06(2016)101